HIV-1 Vpr-induced DNA damage activates NF-κB through ATM-NEMO independent of cell cycle arrest

Short Title: HIV-induced DNA damage alters cellular transcription

Carina Sandoval[1], Karly Nisson[1], Oliver I. Fregoso[1,2]

[1] Molecular Biology Institute, University of California, Los Angeles, California, USA

[2] Department of Microbiology, Immunology, and Molecular Genetics, University of California, Los Angeles, California, USA

Correspondence: Oliver I. Fregoso

Tel: 310.794.1424

Email: ofregoso@mednet.ucla.edu

ABSTRACT

Lentiviral accessory genes enhance replication through diverse mechanisms. HIV-1 accessory protein Vpr modulates the host DNA damage response (DDR) at multiple steps through DNA damage, cell cycle arrest, the degradation of host proteins, and both the activation and repression of DDR signaling. Vpr also alters host and viral transcription; however, the connection between Vpr-mediated DDR modulation and transcriptional activation remains unclear. Here, we determined the cellular consequences of Vpr-induced DNA damage using Vpr mutants that allow us to separate the ability of Vpr to induce DNA damage from cell cycle arrest and other DDR phenotypes including host protein degradation and repression of DDR. RNA-sequencing of cells expressing Vpr or Vpr mutants identified that Vpr alters cellular transcription through mechanisms both dependent and independent of cell cycle arrest. In tissue-cultured U2OS cells and primary human monocyte-derived macrophages (MDMs), Vpr-induced DNA damage activates the ATM-NEMO pathway and alters cellular transcription via NF-κB/RelA signaling. HIV-1 infection of primary MDMs validated Vpr-dependent NF-κB transcriptional activation during infection. Both virion delivered and *de novo* expressed Vpr induced DNA damage and activated ATM-NEMO dependent NF-κB transcription, suggesting that engagement of the DDR and transcriptional reprogramming can occur during early and late stages of viral replication. Together, our data identifies a mechanism by which Vpr activates NF-κB through DNA damage and the ATM-NEMO pathway, which occur independent of cell cycle arrest. We propose this is essential to overcoming restrictive environments, such as in macrophages, to enhance viral transcription and replication.

38 **IMPORTANCE**

39 The HIV accessory protein Vpr is multi-functional and required for viral replication *in vivo*, yet how
40 Vpr enhances viral replication is unknown. Emerging literature suggests that a conserved function
41 of Vpr is engagement of the host DNA damage response (DDR). For example, Vpr activates DDR
42 signaling, causes DDR-dependent cell cycle arrest, promotes degradation of various DDR
43 proteins, and alters cellular consequences of DDR activation. However, a central understanding
44 of how these phenotypes connect and how they affect HIV-infected cells remains unknown. Here,
45 we found that Vpr-induced DNA damage alters the host transcriptome by activating an essential
46 transcription pathway, NF-κB. This occurs early during infection of primary human immune cells,
47 suggesting NF-κB activation and transcriptome remodeling are important for establishing
48 productive HIV-1 infection. Together, our study provides novel insights into how Vpr alters the host
49 environment through the DDR, and what roles Vpr and the DDR play to enhance HIV replication.
50

51 **INTRODUCTION**

52

53 The DDR is a signaling cascade activated in response to exogenous and endogenous genotoxic
54 stressors, such as DNA breaks. The DDR consists of sensor proteins that sense the damaged
55 DNA, transducer proteins that transmit the signal of damaged DNA, and effector proteins that
56 elicit a cellular response. Typically, the DDR is divided into three main pathways based on the
57 mediator kinases activated: Ataxia telangiectasia and Rad3 related (ATR), ataxia telangiectasia
58 mutated (ATM), and DNA-dependent protein kinase (DNA-PK). Single-strand DNA breaks (SSBs)
59 are primarily sensed by RPA to activate ATR signaling, while double-strand DNA breaks (DSBs)
60 can be sensed by the MRN (MRE11, RAD51, and NBS1) or Ku70/80 complexes to activate either
61 ATM or DNA-PK signaling, respectively (1,2). However, a significant amount of crosstalk exists
62 between these pathways. DDR signaling leads to various cellular responses, such as DNA repair,
63 cell cycle arrest (3), transcriptional changes (4,5), apoptosis, or senescence (6).

64

65 Many diverse RNA and DNA viruses have evolved to modulate the DDR to enhance viral
66 replication (7,8). Primate lentiviruses, such as HIV-1, primarily engage the DDR through the
67 accessory protein Vpr (9,10). Vpr is evolutionarily conserved by extant primate lentiviruses and is
68 both delivered by the incoming virion, allowing it to act early in viral replication, and expressed *de*
69 *novo* from the integrated provirus, allowing it to act later in viral replication (11). Viruses lacking
70 Vpr have no appreciable replication defects in T cells and most transformed cell lines, however
71 Vpr is required for replication *in vivo* (12,13) and viruses lacking Vpr have decreased proviral
72 transcription in monocyte derived macrophages (MDMs) (13,14) and dendritic cells (14). This
73 suggests an important role for Vpr in viral transcription. Moreover, studies of Vpr orthologs and
74 mutants in isolation, whether overexpressed or delivered by virus-like particles (VLPs), identified
75 that Vpr engages the host DDR at multiple, potentially unique, steps.

76

77 For example, ATR activation by Vpr leads to cell cycle arrest and requires recruitment of the
78 $CRL4A^{DCAF1}$ complex, which has a primary role in DNA repair (15). $CRL4A^{DCAF1}$ complex
79 recruitment by Vpr also leads to the degradation of many host proteins involved in the DDR (18-
80 27) and is required for Vpr-mediated repression of DSB repair (16). In contrast, we have
81 previously shown that the ability of Vpr to induce DNA damage does not correlate with ATR
82 activation, cell cycle arrest, or repression of DSB repair (16), suggesting that Vpr-induced DNA
83 damage may have unique roles in enhancing lentiviral replication.

84

85 Vpr, DNA damage, and proviral transcription are connected through NF-κB in that both Vpr and
86 DNA damage promote transcriptional changes involving NF-κB (17,18), which is an essential
87 transcription factor for HIV-1 proviral transcription(19,20). In response to DSBs, ATM signaling
88 promotes NF-κB transcriptional upregulation through the ATM-NEMO pathway (21). ATM and
89 NEMO interact in the nucleus before translocating to the cytoplasm (22,23) to subsequently

90 activate RelA nuclear translocation, promoter binding, and NF-κB transcriptional activation.
91 Previous literature suggests that HIV-1 Vpr activates and represses NF-κB pathways through
92 phosphorylation and ubiquitylation of TAK1 to enhance NF-κB signaling (24) and altering the
93 availability of the NF-κB p50-RelA heterodimer to inhibit NF-κB signaling (25), respectively. This
94 proposes a testable model where Vpr-induced DNA damage alters the cellular environment to
95 enhance viral replication by altering transcription through ATM-NEMO and NF-κB. Here, we aimed
96 to identify the cellular consequences of Vpr-induced DNA damage and the connection between
97 DNA damage and ATM activation, cell cycle arrest, and transcriptional changes.
98
99 To determine the consequences of Vpr-induced DNA damage on cellular transcription, we used
100 previously described Vpr mutants that allow us to uncouple DNA damage from the large-scale
101 cellular changes caused by cell cycle arrest. We found that virion-associated or *de novo*
102 expressed Vpr does not require cell cycle arrest to induce DNA breaks and activate DDR signaling
103 in U2OS tissue-culture cells and primary human MDMs. RNA-sequencing (RNA-seq) identified
104 that wild-type HIV-1 Vpr and Vpr mutants that do not induce cell cycle arrest still alter NF-κB
105 associated cellular transcription. In support of this, we showed that Vpr proteins that induce DNA
106 damage activate RelA nuclear translocation and upregulate NF-κB target genes, such as BIRC3
107 and CXCL8. We further assessed the requirement for ATM and NEMO signaling in Vpr-mediated
108 NF-κB activation in U2OS cells and primary human MDMs. We found that Vpr-induced DNA
109 damage activates canonical ATM signaling, and that inhibition of NEMO resulted in loss of NF-κB
110 transcriptional upregulation. HIV-1 infection and virus-like particle (VLP) delivery of Vpr in MDMs
111 validated the Vpr-dependent upregulation of NF-κB target genes early during infection. Together,
112 our data support a model where Vpr-induced DNA damage activates NF-κB through the ATM-
113 NEMO pathway, independent of cell cycle arrest and associated phenotypes. This study further
114 informs how lentiviral accessory proteins engage the DDR at multiple and unique steps, and

115 clarifies how this engagement remodels the host environment and immune pathways to promote
116 viral replication.
117
118 **RESULTS**
119
120 **HIV-1 Vpr alters cellular transcription independent of cell cycle arrest**
121 Given the connections between the DDR and cellular transcription, we set out to understand
122 whether the ability of Vpr to induce DNA damage alters cellular transcription, and whether these
123 transcriptional changes are distinct from those caused by Vpr-mediated cell cycle arrest. To do
124 this, we leveraged a subset of previously established HIV-1 Vpr mutants that inhibit Vpr-mediated
125 cell cycle arrest: Q65R, H71R, and S79A (all generated in the transmitted founder HIV-1 Q23-17
126 background (16)). These mutants have often been used interchangeably throughout the Vpr
127 literature; however, they have not been fully characterized in the same system. We therefore first
128 evaluated the ability of HIV-1 Q23-17 Vpr wild type (WT) and mutants to induce DNA damage,
129 activate DDR signaling, cause cell cycle arrest, and interact with DCAF1 (through which Vpr binds
130 the $CRL4A^{DCAF1}$ E3 ubiquitin ligase complex (26)), as well as their subcellular localization. U2OS
131 cells were infected with a recombinant adeno-associated virus (rAAV) expressing either HIV-1
132 Q23-17 Vpr WT or mutants(10,16) (Fig. S1A). We confirmed that all mutants lost the ability to
133 cause cell cycle arrest (Fig. S1B), as has been previously described(16,27–29). DNA damage
134 was assessed by the comet assay while DDR activation was assessed by immunofluorescence
135 24 hours post infection. Consistent with our previous results (16), HIV-1 Vpr WT and S79A induce
136 DNA breaks (Fig. 1A) and activate the DDR marker γH2A.x (Fig. 1B), while Q65R does not. In
137 addition, we found that H71R induces DNA breaks (Fig. 1A) and activates γH2A.x (Fig. 1B) at
138 levels similar to Vpr WT. Only the H71R mutant is proposed to lose interaction with the DCAF1
139 component of the $CRL4A^{DCAF1}$ E3 ubiquitin ligase complex and thus lose the ability to cause cell
140 cycle arrest and degrade host proteins (16,30–32). In our hands, HIV-1 Q23-17 Vpr WT and S79A

141 recruit similar amounts of DCAF1, H71R recruits a decreased amount of DCAF1 when compared
142 to Vpr WT and S79A, and Q65R recruits background levels of DCAF1 (Fig. S1C). Finally, we
143 found that all Vpr mutants except for Vpr Q65R show similar subcellular localization as WT Vpr
144 (Fig. S1D). Together, our data indicate that, when compared to WT Vpr, Vpr S79A can be used to
145 assess the aspects of Vpr phenotypes that are specific to cell cycle arrest, Vpr H71R can be used
146 to assess those aspects specific to cell cycle arrest and diminished DCAF1 recruitment, and Vpr
147 Q65R can be used as a functionally dead control as it has lost all Vpr-associated phenotypes
148 (Table 1).
149
150 We next asked if Vpr mutants that induce DNA damage in the absence of cell cycle arrest (H71R
151 and S79A) alter the cellular transcriptome. U2OS cells were infected with rAAV expressing HIV-1
152 Vpr WT, H71R, S79A, or Q65R, and RNA was collected at 12, 24, and 36 hours post infection for
153 analysis by bulk RNA-sequencing (RNA-seq). Vpr WT, H71R, and S79A significantly altered
154 cellular transcription 36 hours post infection when compared to empty vector or untreated cells,
155 while Q65R was indistinguishable from empty vector or untreated cells (Fig. 1C-E, Fig. S2A-B,
156 and Supplemental Files S1 & S2). The largest effect on cellular transcription was seen with Vpr
157 WT (950 differentially expressed genes, $Log_2(2)$ fold change p-value < 0.004 and FDR < 0.01),
158 while H71R and S79A showed an intermediate effect (361 differentially expressed genes,
159 $Log_2(1.35)$ p-value < 0.0007 and FDR < 0.01 and 233 differentially expressed genes, $Log_2(1.5)$ p-
160 value < 0.0008 and FDR < 0.006), respectively. All cutoffs failed to identify significant differentially
161 expressed genes in cells expressing Vpr Q65R, empty vector or untreated cells. These data
162 suggest that Vpr the alters cellular transcriptome via mechanisms that are dependent and
163 independent of cell cycle arrest.
164
165 We focused on genes differentially expressed among Vpr WT, H71R, and S79A, as these genes
166 are indicative of changes in cellular transcription that occur independent of cell cycle arrest and

167 are potentially altered by Vpr-induced DNA damage. Out of the top 200 differentially expressed
168 genes for each condition, 68 genes with p-value < 0.01 and FDR < 4.50E-05 were shared among
169 Vpr WT, H71R, and S79A, while 100 additional genes were shared by two out of three conditions
170 (Fig. 1D and 1E, Supplemental Files S1 & S2). Gene ontology (Fig. 1F) and Transcriptional
171 Regulatory Relationships Unraveled by Sentence-based Text-mining (TRRUST)(33) (Fig. 1G)
172 analyses of shared upregulated genes identified that Vpr WT, S79A, and H71R mutants were
173 significantly enriched for positive regulation of RelA/NF-κB signaling and NF-κB signaling
174 pathways (Fig. 1F-G, Fig. S2 A-B and Supplemental Files S1 & S2). TRRUST analysis further
175 identified upregulation of transcription factors that bind and activate the HIV-1 LTR, such as
176 CEBPB (34), SP1 (35), and JUN (36), as well as HDAC1, which modifies the HIV-1 LTR directly
177 (37) (Fig. 1G). Moreover, Protein-protein Interaction Enrichment Analysis of the shared
178 differentially expressed genes identified that Vpr downregulates expression of histones belonging
179 to the H2A, H2B, H4, and H1 family that are involved in nucleosome assembly and DNA
180 Damage/Telomere Stress Induced Senescence (Fig. S2C); consistent with previous literature that
181 Vpr modulates components of the chromatin environment (Romani, Johnson). Collectively, our
182 data show that Vpr alters cellular transcription in the absence of cell cycle arrest and suggest that
183 Vpr-induced DNA damage robustly activates RelA/NF-κB-mediated signaling.
184

185 **HIV-1 Vpr-induced DNA damage activates RelA and promotes NF-κB transcription**

186 Given NF-κB signaling was the strongest upregulated pathway by Vpr WT, H71R, and S79A
187 mutants, that NF-κB signaling is activated by DNA damage, and the precedence for Vpr-mediated
188 modulation of NF-κB (24), we next directly assayed whether Vpr activates RelA/NF-κB in the
189 absence of cell cycle arrest. We focused on H71R because it has lost the ability to cause cell
190 cycle arrest and has diminished DCAF1 binding and host protein degradation (30–32), but
191 maintains the ability to induce DNA damage and activate DDR signaling. NF-κB activation was
192 first validated by qRT-PCR for two NF-κB target genes identified in our RNA-seq, BIRC3 and

193 CXCL8 (Fig. 1E), which play important roles in innate immunity and cell survival (38,39). U2OS
194 cells were infected with rAAV expressing Vpr WT, H71R, and Q65R for 24 or 36 hours. Consistent
195 with the RNA-seq, Vpr WT and H71R upregulate BIRC3 and CXCL8 compared to untreated cells
196 or Q65R mutant at 36hpi (Fig. 2A). To directly assess NF-κB activation, we assayed for RelA
197 localization by immunofluorescence. As RelA is cytoplasmic when inactive and nuclear when
198 active, we expect that Vpr WT and H71R will lead to nuclear translocation of RelA. Indeed, we
199 found that Vpr WT and H71R activate nuclear translocation of RelA similar to the positive control,
200 etoposide, while Vpr Q65R and empty vector do not (Fig 2B). These data demonstrate that Vpr
201 activates RelA and NF-κB transcription in the absence of cell cycle arrest, suggesting that Vpr-
202 induced DNA damage is sufficient to drive NF-κB activation.
203
204 **HIV-1 Vpr-induced DNA damage activates ATM-NEMO signaling**
205 NF-κB is activated in response to many pathways and signals involved in DNA repair and innate
206 immunity (40). One such pathway is ATM-NEMO, where ATM stimulates NEMO to activate RelA
207 and thus NF-κB signaling (23). Previous work has shown that Vpr activates markers of both ATR
208 and ATM signaling (16,41). While ATR is required for Vpr-induced cell cycle arrest, the extent to
209 which Vpr activates ATM and the cellular consequences of ATM activation without cell cycle arrest
210 are unclear. We hypothesized that Vpr-induced DNA damage activates the ATM-NEMO pathway,
211 which consequently promotes RelA/NF-κB transcription.
212
213 To determine if Vpr-induced DNA damage activates ATM signaling in the absence of cell cycle
214 arrest, we measured activation and colocalization of the DNA damage sensors NBS1 and MRE11
215 and the downstream signaling transducers, 53BP1 and γH2A.x. U2OS cells stably expressing
216 NBS1-GFP or 53BP1-GFP (42,43) were infected with rAAV expressing Vpr WT, H71R, and Q65R
217 and DDR activation was assessed through live-cell imaging over 56 hours. We found that Vpr WT
218 and H71R promote the formation of NBS1 and 53PB1 foci similar to the positive control etoposide,

219 while the non-functional Q65R Vpr mutant was indistinguishable from untreated control cells (Fig.
220 3A and Fig. S3A-C). Moreover, both damage sensors, MRE11 and NBS1, and transducers,
221 53PB1 and γH2A.x, colocalize in Vpr WT and H71R similar to etoposide treated cells (Fig. 3B&C).
222 This suggests that Vpr-induced DNA damage activates, but does not dysregulate, classical ATM
223 signaling.
224
225 To determine if NEMO is required for Vpr to upregulate NF-κB transcription, we asked whether
226 Vpr could upregulate NF-κB target genes BIRC3 and CXCL8 when NEMO was absent or
227 inhibited. U2OS parental and NEMO knockout cells (44) were infected with rAAV expressing Vpr
228 WT and mutants (Fig. S4A). In the absence of NEMO, Vpr WT and H71R, but not Q65R, still
229 activated the DDR, indicating NEMO is not required for Vpr-induced DDR signaling (Fig. 4A and
230 Fig. S4B). As expected, NEMO knockout inhibited TNFα and etoposide-induced TNFα
231 expression, confirming loss of NEMO function (Fig. 4B). In the absence of NEMO, Vpr WT and
232 H71R lost the ability to upregulate BIRC3 and CXCL8 (Fig 4C), suggesting that NEMO is required
233 for Vpr-induced NF-κB signaling. To further confirm this observation, we inhibited NEMO using a
234 cell-permeable NEMO binding domain (NBD) inhibitor peptide (1). Similar to NEMO knockout
235 cells, NBD peptide, but not a cell permeable peptide negative control, inhibited TNFα expression
236 following TNFα or etoposide treatment (Fig. 4D). To assess whether NBD peptide inhibited Vpr-
237 induced NF-κB activation, U2OS cells were pretreated with NBD peptide and infected with rAAV
238 expressing Vpr WT and mutants. Consistent with NEMO knockout, the NBD peptide inhibited
239 upregulation of BIRC3 and CXCL8 by Vpr WT and H71R (Fig. 4E), and this inhibition was
240 indistinguishable from loss of NEMO (Fig. S4C). Together, this data suggests that Vpr requires
241 NEMO activation to upregulate transcription of NF-κB target genes.
242
243 **Virion delivered HIV-1 Vpr activates ATM-NEMO NF-κB signaling in primary MDMs**

244 Together our data proposes a model where Vpr-induced DNA damage activates ATM and NEMO
245 signaling, resulting in RelA nuclear translocation and NF-κB transcriptional upregulation. We next
246 tested this model in primary human MDMs (Fig. 5A), where Vpr enhances viral transcription and
247 replication (46). Primary human MDMs (Fig. S5A) were infected with virus-like particles (VLPs)
248 carrying physiological levels of Vpr WT, H71R, or Q65R (Fig. 5B), and assayed for DNA damage,
249 NF-κB activation, and NEMO dependence (Fig. 5A). Similar to overexpression of Vpr in U2OS
250 tissue culture cell lines, VLP-delivered Vpr WT and H71R mutant, but not Q65R or empty VLPs,
251 induced DNA breaks and activated γH2A.x in primary human MDMs (Fig. 5C-D). Consistent with
252 our data in U2OS cells, VLP-delivered Vpr WT and H71R, but not Q65R or empty VLPs,
253 upregulated BIRC3 and CXCL8 similar to the TNFα positive control in primary human MDMs (Fig.
254 5E and Fig. S5B). Finally, NBD peptide delivery prior to VLP infection blocked Vpr WT and H71R-
255 mediated BIRC3 and CXCL8 transcriptional activation, but not Vpr-induced DNA damage in
256 primary human MDMs (Fig. 5D-E and Fig. S5B). These data indicate that physiological levels of
257 virion-delivered Vpr in primary human MDMs induce DNA damage that activates NF-κB
258 transcription in a NEMO dependent manner.
259
260 To determine if HIV-1 infection activates NF-κB target genes, we infected primary human MDMs
261 from four different donors with HIV-1 ΔEnv and assayed for transcriptional changes at early (8
262 hours), intermediate (16 hours), and late (24 and 48 hours) timepoints post infection. HIV-1
263 infection was monitored by flow cytometry for HIV-1 core proteins and qRT-PCR for unspliced
264 HIV-1 genomic transcripts (Fig. S6A-B), while NF-κB activation was measured by qRT-PCR for
265 CXCL8 and BIRC3. HIV-1 ΔEnv infection resulted in upregulation of CXCL8 and BIRC3 in MDMs
266 as early as 8hpi in all donors, despite some donor-to-donor variability in the magnitude of
267 upregulation (Fig. 6A and Fig. S6C), suggesting that HIV-1 infection upregulates NF-κB target
268 genes early during infection, consistent with VLP delivery of Vpr.
269

270 To test whether Vpr was responsible for the upregulation of NF-κB target genes early during HIV-
271 1 ΔENV infection, we generated two additional viruses: HIV-1 ΔVpr and HIV-1 ΔVpr + Vpr
272 packaged in trans (Fig. 6B). We infected primary human MDMs from three additional donors with
273 either HIV-1 ΔENV, HIV-1 ΔENV ΔVpr, HIV-1 ΔENV ΔVpr + Vpr, or mock and assayed for infection
274 and NF-κB activation at 8 hpi. All three viruses infected cells similarly at 8hpi as shown by qRT-
275 PCR for unspliced HIV-1 genomic transcripts (Fig. 6C) and by flow cytometry for HIV-1 core
276 proteins at 48hpi (Fig. S6D). HIV-1 infection upregulated CXCL8 and BIRC3 gene expression,
277 while HIV-1 ΔVpr did not (Fig. 6C and Fig S6E-F). Moreover, upregulation of CXCL8 and BIRC3
278 were rescued by infection of HIV-1 ΔVpr + Vpr (Fig. 6C). These data suggest that Vpr is necessary
279 and sufficient for upregulation of NF-κB target genes early during HIV-1 infection in primary human
280 MDMs. Jointly, our data support a model where both incoming and *de novo* HIV-1 Vpr induce DNA
281 damage that activates ATM-NEMO signaling to upregulate NF-κB transcription (Fig. 7).
282
283 **DISCUSSION**
284
285 In this study, we tested the hypothesis that HIV-1 Vpr alters cellular transcription through induction
286 of DNA damage and activation of DDR signaling. By leveraging Vpr mutants that separate Vpr-
287 induced DNA damage from cell cycle arrest, we identified a current model where Vpr-induced
288 DNA damage activates ATM-NEMO signaling, which stimulates RelA and upregulates NF-κB
289 mediated transcription. Using U2OS and primary human MDMs, the latter of which allowed us to
290 investigate how HIV-1 Vpr engages the DDR in this important cell type for the first time, we
291 showed that Vpr induces DNA breaks and activates markers of ATM signaling independent of cell
292 cycle arrest. Moreover, we showed that Vpr-induced DNA damage correlates with RelA/NF-κB
293 activation, as assayed by bulk RNA-seq, and RelA immunofluorescence. We validated the
294 upregulation of two NF-κB target genes, BIRC3 and CXCL8, and showed that inhibition of NEMO
295 ablates the ability of Vpr to upregulate NF-κB transcription. Finally, VLP delivery of Vpr and HIV-

296 1 infection show that incoming virion-associated Vpr is sufficient to induce DNA damage and
297 activate RelA/NF-κB transcription. In complement, rAAV expression of Vpr show that *de novo*
298 expressed Vpr can also induce DNA damage and activate RelA/NF-κB transcription. These data
299 suggest that Vpr-induced DNA damage can play roles in both early and late stages of viral
300 replication to alter cellular transcription. Overall, our data support a model where Vpr-induced
301 DNA damage activates ATM-NEMO signaling and upregulates RelA/NF-κB transcription in cell
302 lines and primary human MDMs.
303
304 Although Vpr is a multifunctional and enigmatic protein, the DNA damage response is central to
305 many of the phenotypes associated with Vpr. Previous reports from our lab and others have
306 worked to untangle how and why Vpr engages the DDR. A consensus is emerging that Vpr
307 engages the DDR at multiple, potentially unique, steps. Through recruitment of the $CRL4A^{DCAF1}$
308 ubiquitin ligase complex, Vpr degrades various DDR proteins, activates ATR signaling, represses
309 double-strand DNA break repair, and causes cell cycle arrest (16,47). As shown here, Vpr-induced
310 DNA damage directly correlates with NF-κB transcriptional activation that is independent of cell
311 cycle arrest and dependent on ATM signaling. We have demonstrated that Vpr activates markers
312 of ATM signaling, such as MRE11, NBS1, γH2A.x, and 53PB1, in a manner that resembles host
313 activation rather than dysregulation. We have also shown that DNA damage and DDR activation
314 occur in primary human MDMs and with virion-delivered, physiologically relevant levels of Vpr
315 protein. Antagonism or dysregulation of DNA damage sensors through relocalization or
316 sequestration is a conserved mechanism among many viruses to evade innate immune detection
317 (48). While we have shown that Vpr-induced DNA damage activates markers of ATM signaling in
318 a manner that seems to facilitate classical ATM activation, with the end goal of activating
319 transcription, it remains to be seen whether Vpr-mediated activation of ATR, which correlates with
320 $CRL4A^{DCAF1}$ recruitment and cell cycle arrest, is classically activated or dysregulated. Moreover,
321 how Vpr induces DNA breaks leading to both ATM and ATR activation is not understood.

322

323 Complementary studies have shown that Vpr modulates cellular (49) and viral transcription
324 (50,51). In the context of cellular transcription, Vpr activates genes associated with innate
325 immunity and proliferation in CD4+ T cells (52) and promotes the expression of proinflammatory
326 cytokines in MDMs and monocyte-derived dendritic cells (MDDCs) (14,53). Together this
327 suggests that Vpr has a vital role in transcriptional reprogramming to potentially create a
328 proinflammatory environment that is conducive for viral replication. Consistent with these studies,
329 we identified by bulk RNA-seq that Vpr regulates innate immune pathways that are either
330 independent of or dependent on cell cycle arrest.

331

332 Our data also indicate that Vpr activates the RelA/NF-κB immune pathway without induction of
333 cell cycle arrest. This is consistent with previous reports showing that Vpr activates NF-κB
334 transcription via phosphorylation of TAK1 (24), an upstream regulator of NF-κB. We further found
335 that Vpr-induced DNA damage upregulates RelA/NF-κB transcription via ATM-NEMO signaling,
336 adding to the mechanistic understanding of NF-κB activation by Vpr. Through engagement with
337 the $CRL4A^{DCAF1}$ complex, Vpr has also been found to repress NF-κB activation by altering the
338 availability of the NF-κB p50-p65 heterodimer, thus limiting proinflammatory cytokine expression
339 (25). While it remains unclear what differentiates Vpr-mediated NF-κB activation from repression,
340 whether Vpr engages the $CRL4A^{DCAF1}$ complex may be a distinguishing factor. Furthermore, it is
341 clear that in all cases Vpr carefully modulates NF-κB activation without globally activating
342 interferon, which would inhibit viral replication. Thus, further studies understanding how Vpr
343 manages to activate only aspects of NF-κB signaling (54,55) will help to define how Vpr may
344 contribute to the ability of HIV to subvert the innate immune response.

345

346 Although various studies have shown that Vpr also alters viral transcription, the mechanisms are
347 unclear and disparate. For example, Vpr-mediated LTR activation has been associated with cell

348 cycle arrest, as the LTR is most transcriptionally active in G2/M (56,57), the degradation of host
349 proteins such as CCDC137 (58), and CRL4A^{DCAF1} independent mechanisms (59). However, Vpr
350 also promotes LTR transcription in noncycling cells (60,61) where induction of cell cycle arrest is
351 absent and the necessity for degradation of specific host proteins in LTR activation has not been
352 extensively examined. One benefit of Vpr activating NF-κB signaling via ATM is the potential direct
353 enhancement of LTR transcription, as the HIV-1 LTR contains multiple NF-κB binding sites
354 essential for viral gene expression. In addition to NF-κB, we further identified that Vpr activates
355 CEBPB and JUN transcription factors, which have known roles in LTR activation. This potential
356 direct effect on the LTR is similar to Vpr-mediated de-repression of the LTR by removal of the
357 transcriptional repressor ZBTB2 following ATR activation (62). Overall, in the absence of cell cycle
358 arrest, Vpr-induced DNA damage globally alters cellular transcription and upregulates NF-κB
359 signaling and transcription factors that promote LTR-driven transcription, suggesting that Vpr-
360 induced DNA damage is also important for promoting LTR transcription to enhance viral
361 replication.
362
363 Together, our data suggest that during HIV infection incoming Vpr and *de novo* expressed Vpr
364 prime the cellular environment by activating RelA/NF-κB signaling to promote transcription and
365 enhance viral replication in macrophages. Our data align with the growing body of literature that
366 supports the role of accessory proteins to modulate the host environment and the DDR to promote
367 viral replication.

368 **MATERIALS AND METHODS**

369

370 **Plasmids**

371 pcDNA-3xFLAG-Vpr and pscAAV-mCherry-T2A-Vpr WT and mutant plasmids were generated as
372 previously described (16). For rAAV production, pHelper and pAAV-2.5 capsid plasmids were
373 used (Addgene and (16). For VLP production, psPAX2 and pmD2.G were used (Addgene). For
374 HIV-1 ΔENV production, Bru-GFP ΔENV was generated as previously described (63) with
375 pmD2.G (Addgene).

376

377 **Generation of Viruses**

378 rAAV vectors packaging the pscAAV-mCherry-T2A-Vpr WT or mutant plasmids were generated
379 by transient transfection of HEK 293 cells using polyethyleneimine (PEI) as previously described
380 (64). Virus-like particles (VLPs) packaging Vpr WT or mutant proteins were generated by transient
381 transfection of HEK 293T cells using TransIT-LT1 (Mirus). VLPs were harvested 48 hrs post
382 transfection, concentrated through a 25% sucrose cushion at 24,000 rpm for 3 hrs at 4˚C, and
383 resuspended in PBS. Protein packaging was validated through western blot. HIV-1 ΔENV
384 pseudotyped with VSV-G were generated by transient transfection of HEK 293T cells using
385 TransIT-LT1 (Mirus). For HIV-1 ΔENV ΔVpr with Vpr WT packaged in trans (HIV-1ΔVpr +Vpr WT),
386 40 µg of pcDNA-3xFLAG-Vpr WT was also co-transfected in producer 293T cells. Virus was
387 collected 48 hrs post media change and filtered through a 0.45 µm PES filter. Viral titer was
388 identified by measuring activity of reverse-transcription through qPCR (65).

389

390 **Cell Lines and Cell Culture**

391 Human bone osteosarcoma epithelial (U2OS), Human embryonic kidney (HEK) 293, and HEK
392 293T cells were cultured as adherent cells directly on tissue culture plastic (Greiner) in Dulbecco's

393 modified Eagle's medium (DMEM) growth medium (high glucose, L-glutamine, no sodium
394 pyruvate; Gibco) with 10% fetal bovine serum (FBS) (Gibco) and 1% penicillin-streptomycin
395 (Gibco) at 37°C and 5% CO_2. All cells were harvested using 0.05% trypsin-EDTA (Gibco). The
396 panel of U2OS cells stably expressing 53BP1-GFP (43) and NBS1-GFP (42) were kindly provided
397 by Claudia Lukas (University of Copenhagen, Denmark). The U2OS parental and NEMO
398 knockout cells were kindly provided by Zhijian J. Chen (University of Texas Southwestern Medical
399 Center). U2OS cells were pretreated with 50 μM of Nemo-Binding inhibitor (NBD) peptide or NBD
400 negative control peptide (Thermo) for 2 hours prior to infection with rAAV or VLPs.
401
402 **Monocyte-Derived Macrophages (MDMs)**
403 Human peripheral blood mononuclear cells (PBMCs) were obtained from human donors at the
404 UCLA/CFAR Virology Core Laboratory. Primary monocytes were isolated from PBMCs by
405 negative selection using the EasySep™ Monocyte Isolation Kit (STEM CELL) and were
406 differentiated into monocyte-derived macrophages (MDMs) by stimulation with 20 ng/mL
407 macrophage colony-stimulating factor (M-CSF) (R&D Systems). MDMs were cultured in Roswell
408 Park Memorial Institute (RPMI) 1640 growth medium (L-Glutamine) with 10% fetal bovine serum
409 (Gibco) at 37°C and 5% CO_2 for 7 days while replenishing media every 3 days.
410
411 **Alkaline Comet Assay**
412 The alkaline comet assay and data analysis was performed as previously described (16), with
413 minor changes. MDMs were infected with VLPs delivering Vpr WT and mutants at equal protein
414 levels or 25 μM Mitomycin C (Cayman). Cells were harvested with Accutase (STEM CELL) at 10
415 hrs post infection and resuspended in 0.5% low-melting-point agarose at 37°C. Images were
416 acquired on the Zeiss Axio Imager Z1. Images were analyzed using the OpenComet plug-in for
417 ImageJ.
418

419 **RNA-sequencing**

420 Total RNA from U2OS cells was isolated using TRIzol® reagent (Invitrogen). RNA integrity was
421 assessed using the Bioanalyzer TapeStation 4200 RNA High Sensitivity (Agilent). Library
422 Preparation was completed using the KAPA mRNA HyperPrep Kit (Illumina) enriching for Poly(A)
423 RNA with magnetic oligo-dT beads and attaching unique dual indexed adapters. Quality control
424 of the library was done with the Bioanalyzer TapeStation 4200 D1000 High Sensitivity (Agilent).
425 RNA was sequenced using the Hiseq3000 1x50 at the UCLA Technology Center for Genomics &
426 Bioinformatics core. Reads were aligned to the Human h38 STAR genome and gene counts were
427 determined using edgeR. $\log_2$ reads per kilobase of transcript per million reads mapped (rpkms)
428 were calculated for samples compared to untreated cells. Heat map was generated using
429 pheatmap hierarchical clustering on z-score log2 rpkms. Gene ontology, Protein-protein
430 Interaction Enrichment Analysis, and TRRUST analysis were done on Metascape.

431

432 **Quantitative Reverse Transcription PCR (qRT-PCR)**

433 Total RNA was isolated using the PureLink™ RNA Mini Kit (Invitrogen). RNA was reverse
434 transcribed using SuperScript IV First-Stand Synthesis System (Invitrogen) with Oligo(dT)
435 primers. qRT-PCR was performed with PowerTrack SYBR Green Master Mix (Thermo Fisher
436 Scientific) on the LightCycler 480 System (Roche) with the following primers (5' to 3') BIRC3
437 AAGCTACCTCTCAGCCTACTTT and CCACTGTTTTCTGTACCCGGA, CXCL8
438 TTTTGCCAAGGAGTGCTAAAGA and AACCCTCTGCACCCAGTTTTC, TNFα
439 CTCTTCTGCCTGCTGCACTTTG and ATGGGCTACAGGCTTGTCACTC, HIV-1 unspliced RNA
440 Genome GCGACGAAGACCTCCTCAG and GAGGTGGGTTGCTTTGATAGAGA, GAPDH
441 CAAGATCATCAGCAATGCCT and AGGGATGATGTTCTGGAGAG, and Vpr
442 AGGCCATGGCTTCATGGATTA and GATCTACCGGGTCCATTCCTG. mRNA levels were
443 quantified by calculating ΔΔCt. Target transcript Ct values were normalized to the Ct value of the

444 housekeeping gene GAPDH followed by calculating fold change to untreated or empty vector
445 treated cells.
446
447 **Live-Cell Imaging**
448 U2OS-53PB1-GFP and U2OS-NBS1-GFP cells were imaged using the IncuCyte S3 Live-Cell
449 Analysis Instrument (Sartorius). Mean Fluorescence Intensity (MFI) was calculated using the
450 Sartorius software. For higher resolution, U2OS-53PB1-GFP and U2OS-NBS1-GFP cells were
451 imaged using the LSM 900. Foci per cell and foci size were analyzed using ImageJ.
452
453 **Immunofluorescence**
454 Cells were plated in 6- or 24-well tissue culture plates (Greiner) and allowed to adhere overnight,
455 then infected with VLP (equal protein expression), rAAV-2.5 (1.4×10^8 copies/well), or etoposide
456 (Sigma). U2OS cells were permeabilized with 0.5% Triton X-100 in PBS at 4°C for 5 min and fixed
457 in 4% PFA for 20 min, MDM cells were permeabilized with 0.1% Saponin (Fisher) in PBS at 4°C
458 for 15 min and fixed in 4% PFA for 15 min. Cells were washed, incubated with blocking buffer (3%
459 BSA, 0.05% Tween 20, and 0.04 NaN_3 in PBS for U2OS cells or 3% FBS in 0.1% Saponin for
460 MDM cells) for 30 min. Cells were probed with appropriate primary antibodies (anti-γH2A.x
461 Ser139, anti-53BP1, or anti-RelA(p65) [Cell Signaling], anti-GFP [Takara], and anti-MRE11
462 [Novous]) and then washed and probed with Alexa Fluor-conjugated secondary antibodies (Life
463 Technologies). Nuclei were stained with diamidino-2-phenylindole (DAPI; Life Technologies).
464 Images were acquired on the LSM 980.
465
466 **Western Blots and Co-immunoprecipitations**
467 Protein was collected from cells as previously described (16). For co-immunoprecipitations, cells
468 were washed with cold phosphate-buffered saline (PBS) and lysed with radioimmunoprecipitation
469 assay (RIPA) buffer (50 mM Tris-HCl [pH 8.0], 200 mM NaCl, 1 mM EDTA, 0.1% SDS, 1% NP-40,

470 0.5% sodium deoxycholate, Benzonase, protease inhibitor) and clarified by centrifugation 15,500
471 × g for 15 min. Immunoprecipitations were performed overnight at 4°C with Dynabeads Protein G
472 beads (Invitrogen) conjugated to mouse anti-FLAG M2 (Sigma-Aldrich). For western blotting,
473 samples were boiled in 4× sample buffer (40% glycerol, 240 mM Tris, pH 6.8, 8% SDS, 0.5% β-
474 mercaptoethanol, and bromophenol blue) in preparation for SDS-PAGE using 12% Bis-Tris
475 polyacrylamide gels and subsequently transferred onto a polyvinylidene difluoride membrane.
476 Membranes were blocked in intercept blocking buffer (Li-COR Biosciences). Immunoblotting was
477 performed using mouse anti-FLAG M2 (Sigma-Aldrich), rabbit anti-Actin (Bethyl), mouse alpha-
478 Tubulin (Sigma), or rabbit anti-DCAF1 (Proteintech) for 1 hr. Blots were incubated with secondary
479 antibodies IRDye 800CW anti-Rabbit and IRDye 680RD anti-Mouse (Li-COR Biosciences) for 1
480 hr and then visualized using the Li-COR Odyssey M (Li-COR Biosciences).
481
482 **HIV-1 ΔEnv Infection**
483 MDMs were plated in 96-well tissue culture plates (Greiner) and allowed to adhere overnight.
484 MDMs underwent spinfection with HIV-1 ΔEnv pseudotyped with VSV-G (HIV-1), HIV-1 ΔEnv ΔVpr
485 pseudotyped with VSV-G (HIV-1 ΔVpr) , HIV-1 ΔEnv pseudotyped with VSV-G packaging Vpr WT
486 (HIV-1 ΔVpr +Vpr WT) or mock at 1200× *g* for 90 min at 37°C. Infection was assessed 48 hours
487 after infection via qRT-PCR and Flow Cytometry.
488
489 **Flow Cytometry**
490 Isolated monocytes and infected MDMs were lifted from tissue culture plates using accutase
491 (STEM CELL). Cells were stained for CD14-FITC, CD45-APC, or CD16-APC (STEM CELL) for
492 30 min at 4°C, washed with PBS, fixed in 4% PFA for 15 min, permeabilized with 0.1% Triton X-
493 100 in PBS at 4°C for 15 min, then washed with PBS. Cells were probed for HIV-1 core antigen-
494 FITC KC57 (Beckman Coulter) for 1 hr at 4°C then washed with PBS and resuspended in FACS
495 buffer (5% FBS in PBS). Events were assessed by flow cytometry on the AttuneNxT (Thermo

496 Fisher Scientific). At least 10,000 events were collected per run. Data was analyzed using FlowJo
497 software.
498
499 **Statistical Analyses**
500 All statistical analyses were performed using GraphPad Prism 9.
501
502 **Data access**
503 The bulk RNA-sequencing data in this publication was deposited in NCBI's Gene Expression
504 Omnibus and can be accessed through GEO series accession number GSE253779
505 (https://www.ncbi.nlm.nih.gov/geo/query/acc.cgi?acc=GSE253779).
506
507 **AUTHOR CONTRIBUTIONS**
508 Conceptualization, C.S. and O.I.F; methodology, C.S. and K.N.; writing original draft C.S and
509 O.I.F; writing, review and editing C.S., K.N., and O.I.F; visualization C.S. and O.I.F.; supervision
510 and funding acquisition O.I.F. All authors have read and agreed to the published version of the
511 manuscript.
512
513 **FUNDING**
514 This work was supported by NIH NIAID grant R01AI147837 to O.I.F. C.S was supported by NIH
515 NIAID F31 Ruth L. Kirschstein National Research Service Award Predoctoral Fellowship F31-
516 AI165286, and the NIH NIGMS Grant GM007185 T32 Ruth L. Kirschstein National Research
517 Service Award Cell and Molecular Biology Training Grant. K.N. was supported by NIH NIAID
518 AI007323 T32 Ruth L. Kirschstein National Research Service Award. The funders had no role in
519 study design, data collection and interpretation, or the decision to submit the work for publication.
520
521 **ACKNOWLEDGEMENTS**

522 We like to thank Dr. Julia Mack and Julianne Ashby for their assistance and expertise with Live-
523 cell imaging using the LSM900. We thank Dr. Alexander Hoffmann and Dr. Diane Lefaudeux for
524 instruction on RNA-seq analysis. We thank Dr. Claudia Lukas for providing U2OS cells that stably
525 express 53PB1-GFP and NBS1-GFP. We thank Dr. Zhijian J. Chen for providing U2OS NEMO
526 knockout cells. We thank Dr. Steven Bensinger for the LightCycler 480 System, Dr. Jesse
527 Zamudio for the Qubit fluorometer, Dr. Peter Bradley for the Zeiss Axio Imager Z1, Dr. Matteo
528 Pellegrini for the TapeStation, Dr. Steve Jacobsen and Dr. Jefferey Long for the LSM980. We
529 thank Dr. Randilea Nichols Doyle and Vivian Yang for providing comments on the manuscript.
530

531 **COMPETING INTERESTS**

532 The author(s) declare(s) they have no competing interests.

533 **REFERENCES**

534 1. Blackford AN, Jackson SP. ATM, ATR, and DNA-PK: The Trinity at the Heart of the DNA
535 Damage Response. Mol Cell. 2017 Jun 15;66(6):801–17.
536 2. Shiloh Y, Ziv Y. The ATM protein kinase: regulating the cellular response to genotoxic
537 stress, and more. Nat Rev Mol Cell Biol. 2013 Apr;14(4):197–210.
538 3. Matthews HK, Bertoli C, de Bruin RAM. Cell cycle control in cancer. Nat Rev Mol Cell
539 Biol. 2022 Jan;23(1):74–88.
540 4. Valerie K, Delers A, Bruck C, Thiriart C, Rosenberg H, Debouck C, et al. Activation of
541 human immunodeficiency virus type 1 by DNA damage in human cells. Nature. 1988
542 May;333(6168):78–81.
543 5. Dunphy G, Flannery SM, Almine JF, Connolly DJ, Paulus C, Jønsson KL, et al. Non-
544 canonical Activation of the DNA Sensing Adaptor STING by ATM and IFI16 Mediates NF-κB
545 Signaling after Nuclear DNA Damage. Mol Cell. 2018 Sep 6;71(5):745-760.e5.
546 6. Gorgoulis V, Adams PD, Alimonti A, Bennett DC, Bischof O, Bishop C, et al. Cellular
547 Senescence: Defining a Path Forward. Cell. 2019 Oct 31;179(4):813–27.
548 7. Ryan EL, Hollingworth R, Grand RJ. Activation of the DNA Damage Response by RNA
549 Viruses. Biomolecules. 2016 Jan 6;6(1):2.
550 8. Weitzman MD, Fradet-Turcotte A. Virus DNA Replication and the Host DNA Damage
551 Response. Annu Rev Virol. 2018 Sep 29;5(1):141–64.
552 9. Tachiwana H, Shimura M, Nakai-Murakami C, Tokunaga K, Takizawa Y, Sata T, et al.
553 HIV-1 Vpr Induces DNA Double-Strand Breaks. Cancer Res. 2006 Jan 15;66(2):627–31.
554 10. Fregoso OI, Emerman M. Activation of the DNA Damage Response Is a Conserved
555 Function of HIV-1 and HIV-2 Vpr That Is Independent of SLX4 Recruitment. Prasad VR, editor.
556 mBio. 2016 Nov 2;7(5):e01433-16.

557 11. Paxton W, Connor RI, Landau NR. Incorporation of Vpr into human immunodeficiency
558 virus type 1 virions: requirement for the p6 region of gag and mutational analysis. J Virol. 1993
559 Dec;67(12):7229–37.
560 12. Lang SM, Weeger M, Stahl-Hennig C, Coulibaly C, Hunsmann G, Müller J, et al.
561 Importance of vpr for infection of rhesus monkeys with simian immunodeficiency virus. J Virol.
562 1993 Feb;67(2):902–12.
563 13. Beaumont T, Van Nuenen A, Broersen S, Blattner WA, Lukashov VV, Schuitemaker H.
564 Reversal of Human Immunodeficiency Virus Type 1 IIIB to a Neutralization-Resistant Phenotype
565 in an Accidentally Infected Laboratory Worker with a Progressive Clinical Course. J Virol. 2001
566 Mar;75(5):2246–52.
567 14. Miller CM, Akiyama H, Agosto LM, Emery A, Ettinger CR, Swanstrom RI, et al. Virion-
568 Associated Vpr Alleviates a Postintegration Block to HIV-1 Infection of Dendritic Cells. Sundquist
569 WI, editor. J Virol. 2017 Jul;91(13):e00051-17.
570 15. Roshal M, Kim B, Zhu Y, Nghiem P, Planelles V. Activation of the ATR-mediated DNA
571 Damage Response by the HIV-1 Viral Protein R. J Biol Chem. 2003 Jul;278(28):25879–86.
572 16. Li D, Lopez A, Sandoval C, Nichols Doyle R, Fregoso OI. HIV Vpr Modulates the Host
573 DNA Damage Response at Two Independent Steps to Damage DNA and Repress Double-
574 Strand DNA Break Repair. mBio. 2020 Aug 4;11(4):e00940-20.
575 17. Brzostek-Racine S, Gordon C, Van Scoy S, Reich NC. The DNA Damage Response
576 Induces IFN. J Immunol. 2011 Nov 15;187(10):5336–45.
577 18. Roux P, Alfieri C, Hrimech M, Cohen EA, Tanner JE. Activation of Transcription Factors
578 NF-κB and NF-IL-6 by Human Immunodeficiency Virus Type 1 Protein R (Vpr) Induces
579 Interleukin-8 Expression. J Virol. 2000 May 15;74(10):4658–65.
580 19. Gimble JM, Duh E, Ostrove JM, Gendelman HE, Max EE, Rabson AB. Activation of the
581 human immunodeficiency virus long terminal repeat by herpes simplex virus type 1 is

582 associated with induction of a nuclear factor that binds to the NF-kappa B/core enhancer
583 sequence. J Virol. 1988 Nov;62(11):4104–12.
584 20. Rohr O, Marban C, Aunis D, Schaeffer E. Regulation of HIV-1 gene transcription: from
585 lymphocytes to microglial cells. J Leukoc Biol. 2003 Nov 1;74(5):736–49.
586 21. Wu ZH, Shi Y, Tibbetts RS, Miyamoto S. Molecular Linkage Between the Kinase ATM
587 and NF-κB Signaling in Response to Genotoxic Stimuli. Science. 2006 Feb 24;311(5764):1141–
588 6.
589 22. Huang TT, Wuerzberger-Davis SM, Wu ZH, Miyamoto S. Sequential modification of
590 NEMO/IKKgamma by SUMO-1 and ubiquitin mediates NF-kappaB activation by genotoxic
591 stress. Cell. 2003 Nov 26;115(5):565–76.
592 23. Miyamoto S. Nuclear initiated NF-κB signaling: NEMO and ATM take center stage. Cell
593 Res. 2011 Jan;21(1):116–30.
594 24. Liu R, Lin Y, Jia R, Geng Y, Liang C, Tan J, et al. HIV-1 Vpr stimulates NF-κB and AP-1
595 signaling by activating TAK1. Retrovirology. 2014 Jun 9;11(1):45.
596 25. Kogan M, Deshmane S, Sawaya BE, Gracely EJ, Khalili K, Rappaport J. Inhibition of
597 NF-κB activity by HIV-1 Vpr is dependent on Vpr binding protein. J Cell Physiol. 2013
598 Apr;228(4):781–90.
599 26. Zhang S, Feng Y, Narayan O, Zhao LJ. Cytoplasmic retention of HIV-1 regulatory protein
600 Vpr by protein-protein interaction with a novel human cytoplasmic protein VprBP. Gene. 2001
601 Jan;263(1–2):131–40.
602 27. Kawano K, Doucet AJ, Ueno M, Kariya R, An W, Marzetta F, et al. HIV-1 Vpr and p21
603 restrict LINE-1 mobility. Nucleic Acids Res. 2018 Sep 19;46(16):8454–70.
604 28. Vodicka MA, Koepp DM, Silver PA, Emerman M. HIV-1 Vpr interacts with the nuclear
605 transport pathway to promote macrophage infection. Genes Dev. 1998 Jan 15;12(2):175–85.

606 29. Chen M, Elder RT, Yu M, O'Gorman MG, Selig L, Benarous R, et al. Mutational Analysis
607 of Vpr-Induced G_2 Arrest, Nuclear Localization, and Cell Death in Fission Yeast. J Virol. 1999
608 Apr;73(4):3236–45.
609 30. Mansky LM, Le Rouzic E, Benichou S, Gajary LC. Influence of Reverse Transcriptase
610 Variants, Drugs, and Vpr on Human Immunodeficiency Virus Type 1 Mutant Frequencies. J
611 Virol. 2003 Feb;77(3):2071–80.
612 31. Hrecka K, Hao C, Shun MC, Kaur S, Swanson SK, Florens L, et al. HIV-1 and HIV-2
613 exhibit divergent interactions with HLTF and UNG2 DNA repair proteins. Proc Natl Acad Sci
614 [Internet]. 2016 Jul 5 [cited 2023 May 11];113(27). Available from:
615 https://pnas.org/doi/full/10.1073/pnas.1605023113
616 32. Yan J, Shun MC, Hao C, Zhang Y, Qian J, Hrecka K, et al. HIV-1 Vpr Reprograms CLR4
617 ^{DCAF1} E3 Ubiquitin Ligase to Antagonize Exonuclease 1-Mediated Restriction of HIV-1 Infection.
618 Smithgall TE, editor. mBio. 2018 Nov 7;9(5):e01732-18.
619 33. Han H, Shim H, Shin D, Shim JE, Ko Y, Shin J, et al. TRRUST: a reference database of
620 human transcriptional regulatory interactions. Sci Rep. 2015 Jun 12;5(1):11432.
621 34. Mameli G, Deshmane SL, Ghafouri M, Cui J, Simbiri K, Khalili K, et al. C/EBPβ regulates
622 human immunodeficiency virus 1 gene expression through its association with cdk9. J Gen
623 Virol. 2007 Feb 1;88(2):631–40.
624 35. Harrich D, Garcia J, Wu F, Mitsuyasu R, Gonazalez J, Gaynor R. Role of SP1-binding
625 domains in in vivo transcriptional regulation of the human immunodeficiency virus type 1 long
626 terminal repeat. J Virol. 1989 Jun;63(6):2585–91.
627 36. Kumar A, Manna SK, Dhawan S, Aggarwal BB. HIV-Tat protein activates c-Jun N-
628 terminal kinase and activator protein-1. J Immunol Baltim Md 1950. 1998 Jul 15;161(2):776–81.
629 37. Coull JJ, Romerio F, Sun JM, Volker JL, Galvin KM, Davie JR, et al. The Human Factors
630 YY1 and LSF Repress the Human Immunodeficiency Virus Type 1 Long Terminal Repeat via
631 Recruitment of Histone Deacetylase 1. J Virol. 2000 Aug;74(15):6790–9.

632 38. Russo RC, Garcia CC, Teixeira MM, Amaral FA. The CXCL8/IL-8 chemokine family and
633 its receptors in inflammatory diseases. Expert Rev Clin Immunol. 2014 May 1;10(5):593–619.
634 39. Frazzi R. BIRC3 and BIRC5: multi-faceted inhibitors in cancer. Cell Biosci. 2021 Jan
635 7;11(1):8.
636 40. Mitchell S, Vargas J, Hoffmann A. Signaling via the NFκB system. WIREs Syst Biol Med.
637 2016 May;8(3):227–41.
638 41. Nakai-Murakami C, Shimura M, Kinomoto M, Takizawa Y, Tokunaga K, Taguchi T, et al.
639 HIV-1 Vpr induces ATM-dependent cellular signal with enhanced homologous recombination.
640 Oncogene. 2007 Jan;26(4):477–86.
641 42. Lukas C, Melander F, Stucki M, Falck J, Bekker-Jensen S, Goldberg M, et al. Mdc1
642 couples DNA double-strand break recognition by Nbs1 with its H2AX-dependent chromatin
643 retention. EMBO J. 2004 Jul 7;23(13):2674–83.
644 43. Bekker-Jensen S, Lukas C, Melander F, Bartek J, Lukas J. Dynamic assembly and
645 sustained retention of 53BP1 at the sites of DNA damage are controlled by Mdc1/NFBD1. J Cell
646 Biol. 2005 Jul 18;170(2):201–11.
647 44. Du M, Ea CK, Fang Y, Chen ZJ. Liquid phase separation of NEMO induced by
648 polyubiquitin chains activates NF-κB. Mol Cell. 2022 Jul;82(13):2415-2426.e5.
649 45. Strickland I, Ghosh S. Use of cell permeable NBD peptides for suppression of
650 inflammation. Ann Rheum Dis. 2006 Nov;65(Suppl 3):iii75–82.
651 46. Mashiba M, Collins DR, Terry VH, Collins KL. Vpr Overcomes Macrophage-Specific
652 Restriction of HIV-1 Env Expression and Virion Production. Cell Host Microbe. 2014 Dec
653 10;16(6):722–35.
654 47. Liang Z, Liu R, Lin Y, Liang C, Tan J, Qiao W. HIV-1 Vpr protein activates the NF-κB
655 pathway to promote G2/M cell cycle arrest. Virol Sin. 2015 Dec 1;30(6):441–8.

656 48. Lopez A, Nichols Doyle R, Sandoval C, Nisson K, Yang V, Fregoso OI. Viral Modulation
657 of the DNA Damage Response and Innate Immunity: Two Sides of the Same Coin. J Mol Biol.
658 2022 Mar 30;434(6):167327.
659 49. Virgilio MC, Miguel Disbennett W, Chen T, Lubow J, Welch JD, Collins KL. HIV-1 Vpr
660 combats the PU.1-driven antiviral response in primary human macrophages. BioRxiv Prepr Serv
661 Biol. 2023 Mar 21;2023.03.21.533528.
662 50. Joseph AM, Ladha JS, Mojamdar M, Mitra D. Human immunodeficiency virus-1 Nef
663 protein interacts with Tat and enhances HIV-1 gene expression. FEBS Lett. 2003 Jul 31;548(1–
664 3):37–42.
665 51. Sawaya BE, Khalili K, Gordon J, Taube R, Amini S. Cooperative Interaction between
666 HIV-1 Regulatory Proteins Tat and Vpr Modulates Transcription of the Viral Genome *. J Biol
667 Chem. 2000 Nov 10;275(45):35209–14.
668 52. Bauby H, Ward CC, Hugh-White R, Swanson CM, Schulz R, Goujon C, et al. HIV-1 Vpr
669 Induces Widespread Transcriptomic Changes in CD4 $^{+}$ T Cells Early Postinfection. Goff SP,
670 editor. mBio. 2021 Jun 29;12(3):e01369-21.
671 53. Lv L, Wang Q, Xu Y, Tsao LC, Nakagawa T, Guo H, et al. Vpr Targets TET2 for
672 Degradation by CRL4VprBP E3 Ligase to Sustain IL-6 Expression and Enhance HIV-1
673 Replication. Mol Cell. 2018 Jun 7;70(5):961-970.e5.
674 54. Romero N, Favoreel HW. Pseudorabies virus infection triggers NF-κB activation via the
675 DNA damage response, but actively inhibits NFkB-dependent gene expression. J Virol. 2021
676 Oct 6;JVI.01666-21.
677 55. Harman AN, Nasr N, Feetham A, Galoyan A, Alshehri AA, Rambukwelle D, et al. HIV
678 Blocks Interferon Induction in Human Dendritic Cells and Macrophages by Dysregulation of
679 TBK1. Silvestri G, editor. J Virol. 2015 Jul;89(13):6575–84.

680 56. Gummuluru S, Emerman M. Cell Cycle- and Vpr-Mediated Regulation of Human
681 Immunodeficiency Virus Type 1 Expression in Primary and Transformed T-Cell Lines. J Virol.
682 1999 Jul;73(7):5422–30.
683 57. Goh WC, Rogel ME, Kinsey CM, Michael SF, Fultz PN, Nowak MA, et al. HIV-1 Vpr
684 increases viral expression by manipulation of the cell cycle: A mechanism for selection of Vpr in
685 vivo. Nat Med. 1998 Jan;4(1):65–71.
686 58. Zhang F, Bieniasz PD. HIV-1 Vpr induces cell cycle arrest and enhances viral gene
687 expression by depleting CCDC137. eLife. 9:e55806.
688 59. Nodder SB, Gummuluru S. Illuminating the Role of Vpr in HIV Infection of Myeloid Cells.
689 Front Immunol [Internet]. 2019 [cited 2023 Apr 3];10. Available from:
690 https://www.frontiersin.org/articles/10.3389/fimmu.2019.01606
691 60. Varin A, Decrion AZ, Sabbah E, Quivy V, Sire J, Van Lint C, et al. Synthetic Vpr Protein
692 Activates Activator Protein-1, c-Jun N-terminal Kinase, and NF-κB and Stimulates HIV-1
693 Transcription in Promonocytic Cells and Primary Macrophages*. J Biol Chem. 2005 Dec
694 30;280(52):42557–67.
695 61. Fabryova H, Kao S, Sukegawa S, Miyagi E, Taylor L, Ferhadian D, et al. HIV-1 Vpr
696 Induces Degradation of Gelsolin, a Myeloid Cell-Specific Host Factor That Reduces Viral
697 Infectivity by Inhibiting the Expression and Packaging of the HIV-1 Env Glycoprotein. Goff SP,
698 editor. mBio. 2023 Feb 28;14(1):e02973-22.
699 62. Bruce JW, Bracken M, Evans E, Sherer N, Ahlquist P. ZBTB2 represses HIV-1
700 transcription and is regulated by HIV-1 Vpr and cellular DNA damage responses. PLOS Pathog.
701 2021 Feb 26;17(2):e1009364.
702 63. Yamashita M, Emerman M. Capsid Is a Dominant Determinant of Retrovirus Infectivity in
703 Nondividing Cells. J Virol. 2004 Jun;78(11):5670–8.
704 64. Choi VW, Asokan A, Haberman RA, Samulski RJ. Production of Recombinant Adeno-
705 Associated Viral Vectors for In Vitro and In Vivo Use. Curr Protoc Mol Biol [Internet]. 2007 Apr

706 [cited 2023 May 3];78(1). Available from:
707 https://onlinelibrary.wiley.com/doi/10.1002/0471142727.mb1625s78
708 65. Vermeire J, Naessens E, Vanderstraeten H, Landi A, Iannucci V, Van Nuffel A, et al.
709 Quantification of Reverse Transcriptase Activity by Real-Time PCR as a Fast and Accurate
710 Method for Titration of HIV, Lenti- and Retroviral Vectors. Tachedjian G, editor. PLoS ONE. 2012
711 Dec 5;7(12):e50859.
712

713 **FIGURE LEGENDS**

714

715 **Fig 1: HIV-1 Vpr induces DNA damage and alters cellular transcription independent of cell**
716 **cycle arrest.** (A) Comet assay of U2OS cells infected with rAAV expressing 3xFLAG-tagged Vpr
717 WT, S79A, H71R, Q65R, empty vector (EV) (negative control), or 50uM etoposide (positive
718 control). Percent tail DNA was quantified at 24 hours post infection (hpi) using the OpenComet
719 plug-in for the ImageJ software. Each circle represents one cell. N=3, one representative
720 experiment shown. (B) Representative immunofluorescence images of U2OS cells infected under
721 the same conditions as Fig. 1A; γH2A.x (magenta) and nuclei stained with DAPI (blue). Images
722 were taken at 63x magnification. N=3, one representative experiment shown. (C) RNA-seq of
723 U2OS cells at 36 hpi. Heat map displays Log_2 fold changes of upregulated genes in red and
724 downregulated genes in blue. Each column represents a biological replicate. (D) Venn diagram
725 of the top 100 upregulated and top 100 downregulated genes among Vpr WT, S79A, H71R, and
726 Q65R. (E) Dot plot of the 68 conserved differentially expressed genes among Vpr WT, S79A, and
727 H71R. BIRC3 and CXCL8 are highlighted as the two most upregulated genes (Log_2 fold change)
728 under all conditions. (F) Gene ontology and (G) TRRUST analysis of the 30 upregulated genes
729 performed with Metascape software. Asterisk indicate statistical significance compared to EV
730 control, as determined by one-way ANOVA test (NS, nonsignificant; ** P< 0.001, *** P< 0.0004,
731 **** P< 0.0001). Related to Figures S1 and S2.

732

733 **Fig 2: HIV-1 Vpr activates RelA and promotes NF-κB transcription independent of cell cycle**
734 **arrest.** (A) qRT-PCR validation of upregulated NF-κB target genes BIRC3 and CXCL8.
735 Normalized expression (ΔΔCt) was calculated by normalizing to GAPDH followed by calculating
736 fold change to untreated or empty vector treated cells. Cells treated under the same conditions
737 as Fig. 1C. N=3, one representative experiment shown with technical triplicates. (B)
738 Representative immunofluorescence images of U2OS cells infected under the same conditions

739 as Fig. 1A; RelA (red) and nuclei stained with DAPI (blue). Images were taken at 63x
740 magnification. N=3, one representative experiment shown. Asterisk indicate statistical
741 significance compared to untreated control, as determined by one-way ANOVA test (NS,
742 nonsignificant; *** P< 0.0003, **** P< 0.0001).
743
744 **Fig 3: Vpr-induced DNA damage activates ATM signaling independent of cell cycle arrest.**
745 (A) Live-cell imaging of U2OS cells stably expressing NBS1-GFP or 53PB1-GFP. Cells were
746 infected under the same conditions as Fig. 1A and representative images were taken at 33 hpi at
747 63x magnification. N=3, one representative experiment shown. (B) Representative images of co-
748 localization of DNA damage sensors MRE11 (magenta) and NBS1 (yellow) in U2OS NBS1-GFP
749 or (C) DNA damage transducers γH2A.x (magenta) and 53PB1 (yellow) in U2OS 53PB1-GFP
750 cells infected under the same conditions as Fig. 1A. Images taken at 24 hpi at 63x magnification.
751 N=3, one representative experiment shown. Related to Figure S3.
752
753 **Fig 4: Vpr upregulates NF-κB transcription dependent on NEMO, yet independent of cell**
754 **cycle arrest.** (A) Representative images of U2OS parental or NEMO knockout cells infected with
755 EV or Vpr WT displaying γH2A.x (magenta), Vpr FLAG (yellow), and DAPI (blue). Images taken
756 at 24hpi at 63x magnification. N=3, one representative experiment shown. (B) qRT-PCR of TNFα
757 in U2OS parental or U2OS NEMO knockout cells treated with TNFα or Etoposide (positive
758 controls). RNA was isolated at 36hpi. Asterisk indicate statistical significance compared to U2OS
759 parental cells. (C) qRT-PCR of BIRC3 and CXCL8 in U2OS parental or NEMO knockout cells.
760 Cells were treated under the same conditions as Fig. 1C. N=3, one representative experiment
761 shown with technical triplicates. Asterisk indicate statistical significance compared to U2OS
762 parental cells. (D) qRT-PCR of TNFα in the presence of Nemo-Binding inhibitor peptide (NBD, +)
763 or the NBD negative control peptide (-) at 36 hpi. U2OS cells were pretreated with 50μM of NBD

764 peptide or NBD negative control peptide for 2 hours prior treatment with TNFα or etoposide.
765 Asterisk indicate statistical significance compared to U2OS parental cells. (E) qRT-PCR of BIRC3
766 and CXCL8 in the presence of NBD inhibitor peptide (+) or the NBD negative control peptide (-)
767 at 36 hpi. U2OS cells were pretreated as in Fig. 4D and infected with rAAV expressing 3xFLAG-
768 tagged Vpr WT, H71R, Q65R, EV (negative control). Normalized expression to GAPDH. N=3, one
769 representative experiment shown with technical triplicates. Asterisk indicate statistical
770 significance compared to NBD negative control, as determined by one-way ANOVA test (NS,
771 nonsignificant; ** P< 0.001, *** P< 0.0003, **** P< 0.0001). Related to Figure S4.
772
773 **Fig 5: Vpr-induced DNA damage activates ATM-NEMO signaling and NF-κB transcription**
774 **in primary human MDMs early during infection.** (A) Experimental schematic depicting the
775 isolation and differentiation of primary human monocyte-derived macrophages (MDMs) from
776 peripheral blood mononuclear cells (PBMCs) followed by delivery of Vpr via Virus-like Particles
777 (VLPs). Infected MDMs were assayed for induction of DNA damage, activation of DDR signaling,
778 and the upregulation of NF-κB target genes in the context of NEMO-Binding inhibitor peptide
779 (NBD) or the NBD negative control peptide. (B) Western blot of 3X FLAG-Vpr WT and mutants
780 packaged in VLPs. (C) Comet assay of MDMs treated with VLPs packaging 3xFLAG-tagged Vpr
781 WT, H71R, Q65R, empty VLPs (negative control), or 25uM Mitomycin C (Mito C, positive control)
782 for 8 hours. Comet assay analysis was performed as in Fig. 1A. N=2, one representative
783 experiment shown. (D) Representative immunofluorescence images of MDMs infected with VLPs
784 as in Fig. 5B and treated with the NBD inhibitor peptide (+) or the NBD negative control peptide
785 (-). γH2A.x (magenta) and nuclei stained with DAPI (blue). Images were taken at 100x
786 magnification. N=3, one representative experiment shown. (E) qRT-PCR for CXCL8 of MDMs
787 treated with NBD peptide as in Fig. 5C with TNFα positive control. N=3, one representative
788 experiment shown with technical triplicates. Normalized expression to GAPDH. Asterisk indicate

789 statistical significance compared to NBD negative control, as determined by one-way ANOVA test
790 (NS, nonsignificant; * P<0.03, ** P < 0.005, **** P< 0.0001). Related to Figure S5.
791
792 **Fig 6: Vpr is necessary and sufficient for activation of NF-kB target genes by HIV-1 in**
793 **primary human MDMs.** (A) qRT-PCR for CXCL8 of MDMs infected with HIV-1 ΔEnv for 8, 16,
794 24, and 48 hpi from four separate donors. Normalized expression to GAPDH. (B) Western blot of
795 Vpr packaged in mock, HIV-1, HIV-1 ΔVpr, HIV-1 ΔVpr +Vpr WT viruses. (C) qRT-PCR for
796 unspliced HIV-1 genomic transcripts and CXCL8 from MDMs infected with MOI 5U/mL (RT
797 activity) of HIV-1, HIV-1 ΔVpr, HIV-1 ΔVpr +Vpr WT viruses or mock (negative control). The mean
798 (N=3) of three separate donors is shown. Normalized expression to GAPDH. Asterisk indicate
799 statistical significance compared to mock negative control, as determined by one-way ANOVA
800 (NS, nonsignificant; * P < 0.005). Related to Figure S6.
801
802 **Fig 7: Model showing Vpr-induced DNA damage activates ATM and NEMO signaling**
803 **resulting in RelA nuclear translocation and NF-κB transcriptional upregulation.** 1. Vpr
804 induces double-strand DNA breaks independent of cell cycle arrest. 2. Vpr-induced DNA damage
805 activates markers of ATM signaling including MRE11, NBS1, γH2A.x, and 53PB1. 3. ATM-DDR
806 activation results in NEMO relieving RelA inhibition from inhibitor of NF-κB (IκBα and IκBβ). 4.
807 RelA translocates into the nucleus. 5. RelA binds to NF-κB promoters and activates transcription
808 (txn) of NF-κB target genes such as BIRC3 and CXCL8. (Schematic made on Biorender).

Fig 1.

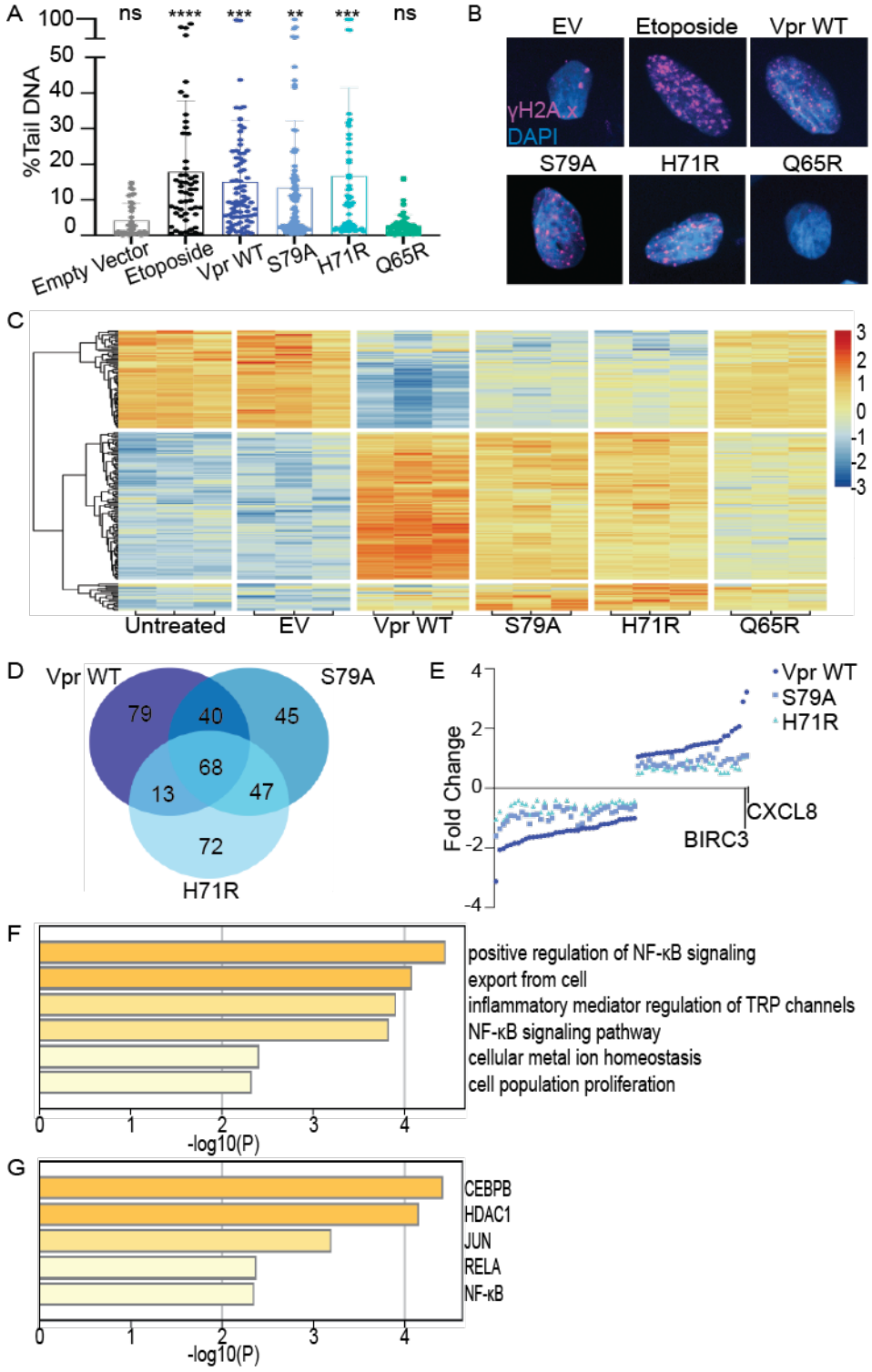
A
ns
****
***
**
***
ns
% Tail DNA
100
50
40
30
20
10
0
Empty Vector
Etoposide
Vpr WT
S79A
H71R
Q65R
B
EV
Etoposide
Vpr WT
γH2A.x
DAPI
S79A
H71R
Q65R
C
Untreated
EV
Vpr WT
S79A
H71R
Q65R
D
Vpr WT
S79A
H71R
79
40
45
68
13
47
72
E
Vpr WT
S79A
H71R
Fold Change
CXCL8
BIRC3
F
positive regulation of NF-κB signaling
export from cell
inflammatory mediator regulation of TRP channels
NF-κB signaling pathway
cellular metal ion homeostasis
cell population proliferation
-log10(P)
G
CEBPB
HDAC1
JUN
RELA
NF-κB
-log10(P)

811 **Fig 2.**

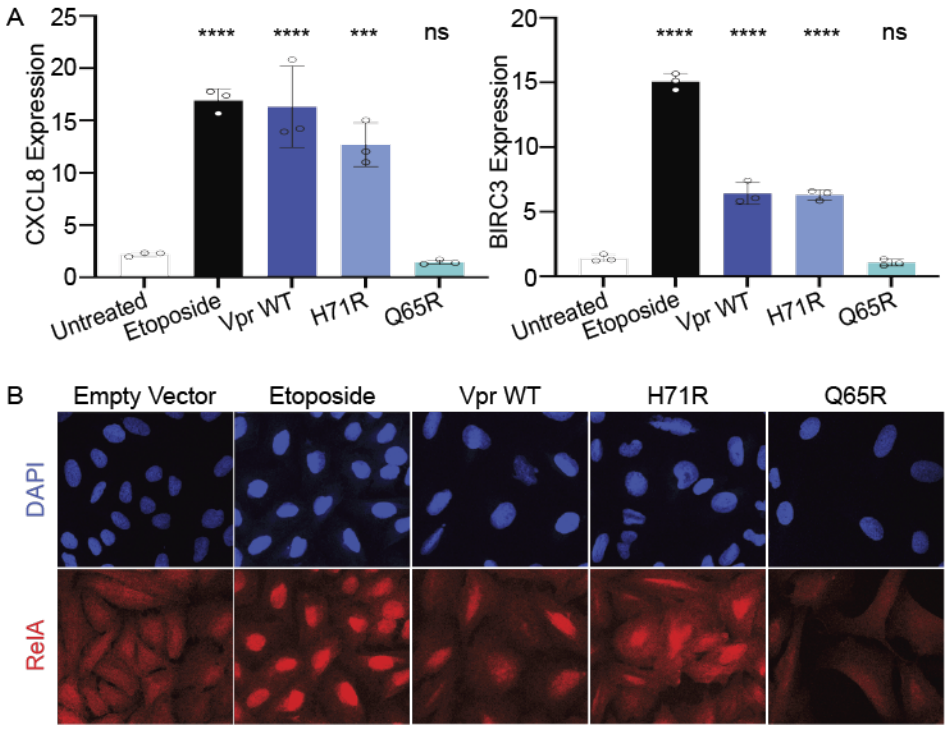
A
CXCL8 Expression
25
20
15
10
5
0
****
****
***
ns
Untreated
Etoposide
Vpr WT
H71R
Q65R
BIRC3 Expression
20
15
10
5
0
****
****
****
ns
Untreated
Etoposide
Vpr WT
H71R
Q65R
B
Empty Vector
Etoposide
Vpr WT
H71R
Q65R
DAPI
RelA

812

813 **Fig 3.**

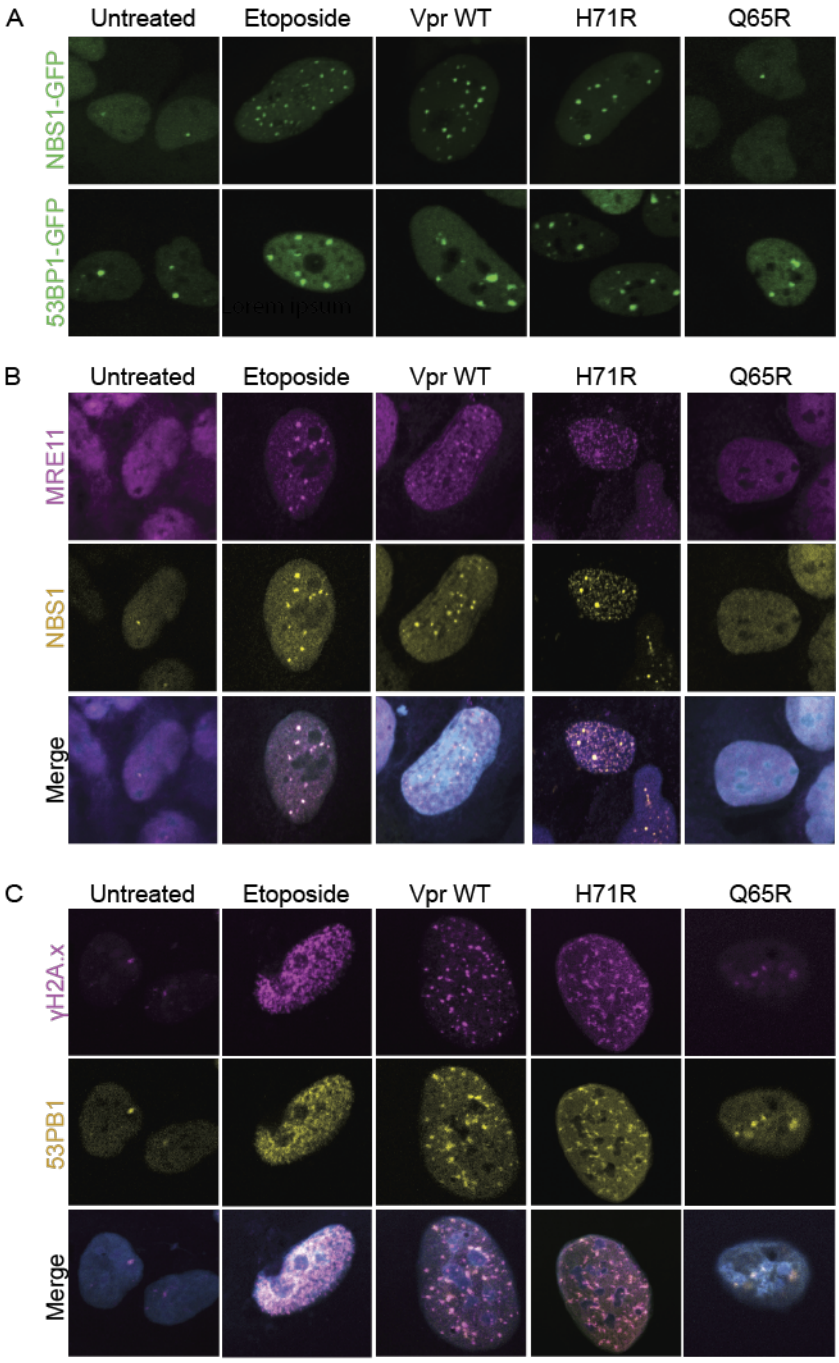
A
Untreated
Etoposide
Vpr WT
H71R
Q65R
NBS1-GFP
53BP1-GFP
B
Untreated
Etoposide
Vpr WT
H71R
Q65R
MRE11
NBS1
Merge
C
Untreated
Etoposide
Vpr WT
H71R
Q65R
γH2A.x
53PB1
Merge

814

Fig 4.

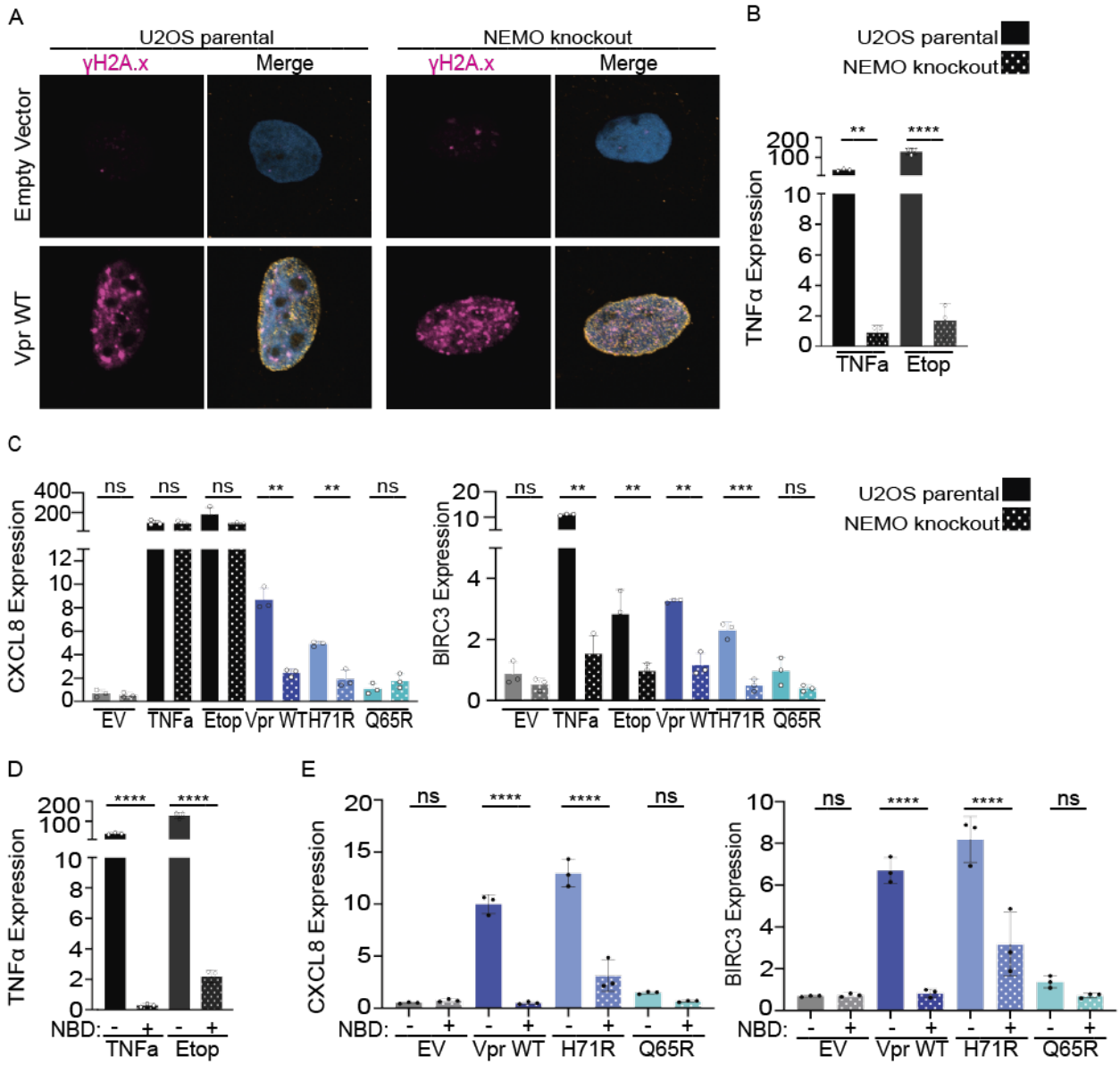
A
U2OS parental
NEMO knockout
γH2A.x
Merge
Empty Vector
Vpr WT
B
U2OS parental
NEMO knockout
TNFα Expression
TNFa
Etop
C
CXCL8 Expression
BIRC3 Expression
EV
TNFa
Etop
Vpr WT
H71R
Q65R
D
TNFα Expression
NBD:
E
CXCL8 Expression
BIRC3 Expression

Fig 5.

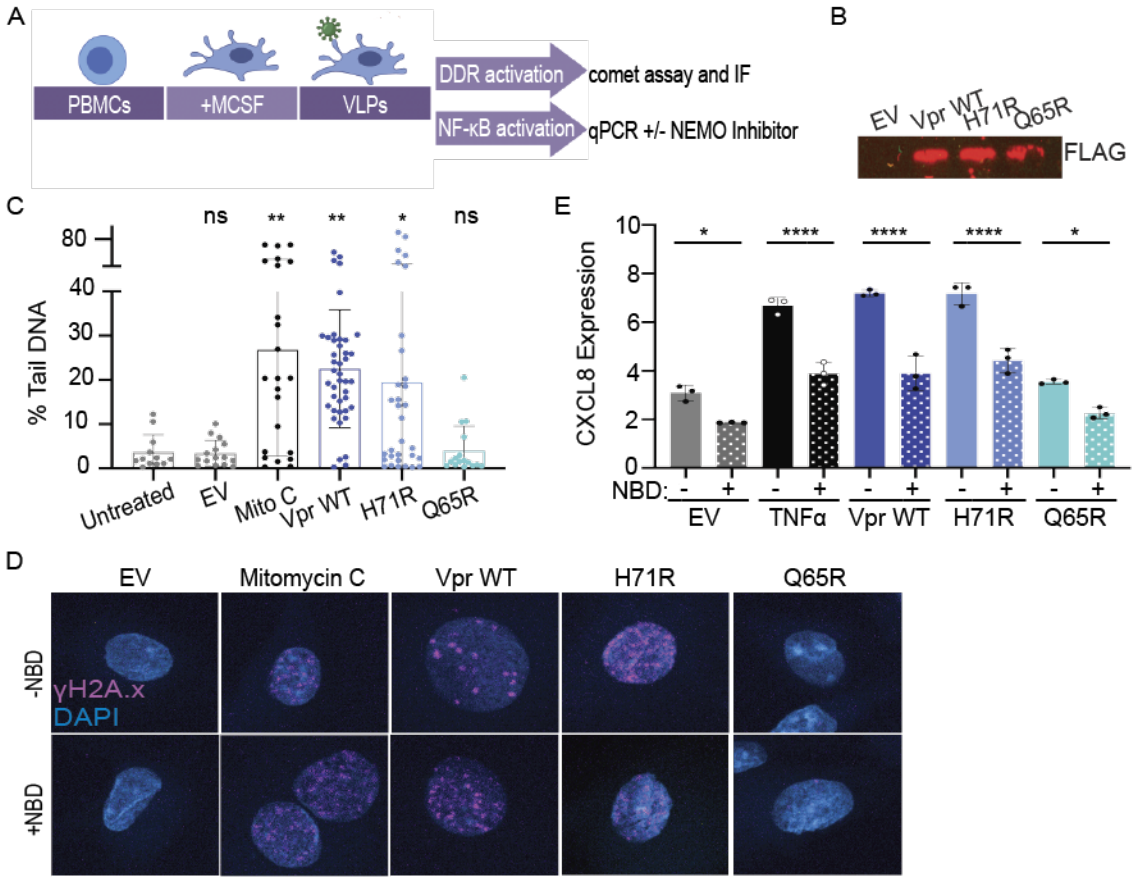
A
PBMCs
+MCSF
VLPs
DDR activation
comet assay and IF
NF-κB activation
qPCR +/- NEMO Inhibitor
B
EV
Vpr WT
H71R
Q65R
FLAG
C
% Tail DNA
ns
**
**
*
ns
Untreated
EV
Mito C
Vpr WT
H71R
Q65R
E
CXCL8 Expression
*
****
****
****
*
NBD:
EV
TNFα
Vpr WT
H71R
Q65R
D
EV
Mitomycin C
Vpr WT
H71R
Q65R
-NBD
+NBD
γH2A.x
DAPI

819 **Fig 6.**

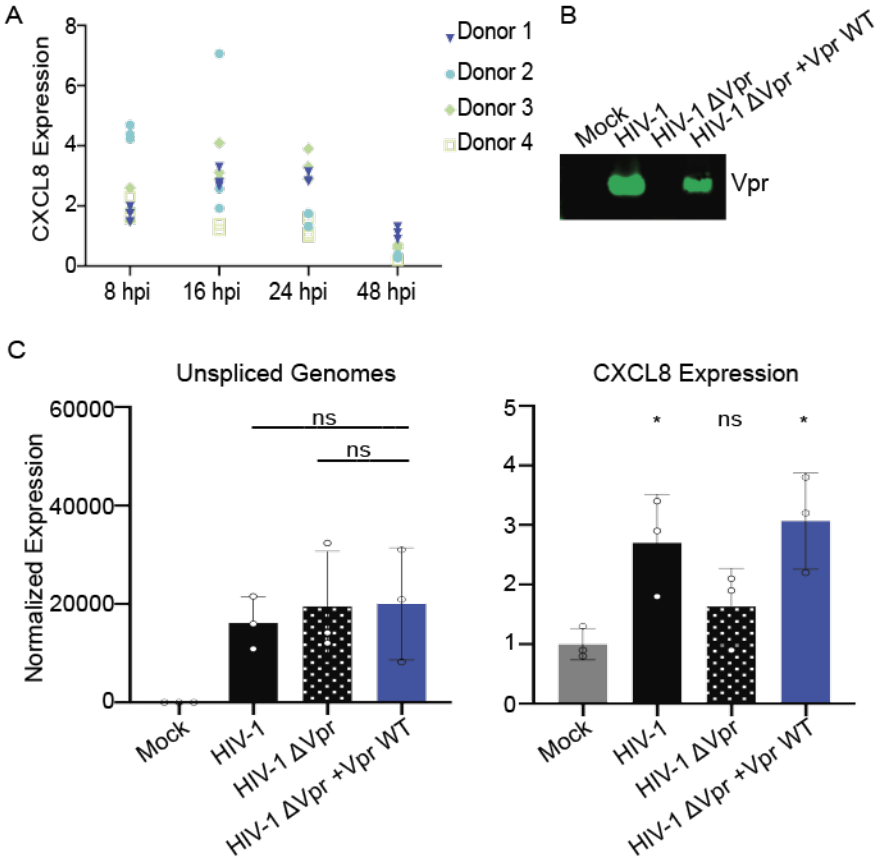
A
CXCL8 Expression
8
6
4
2
0
8 hpi
16 hpi
24 hpi
48 hpi
Donor 1
Donor 2
Donor 3
Donor 4
B
Mock
HIV-1
HIV-1 ΔVpr
HIV-1 ΔVpr +Vpr WT
Vpr
C
Unspliced Genomes
Normalized Expression
60000
40000
20000
0
ns
ns
Mock
HIV-1
HIV-1 ΔVpr
HIV-1 ΔVpr +Vpr WT
CXCL8 Expression
5
4
3
2
1
0
*
ns
*
Mock
HIV-1
HIV-1 ΔVpr
HIV-1 ΔVpr +Vpr WT

820

821 **Fig 7.**

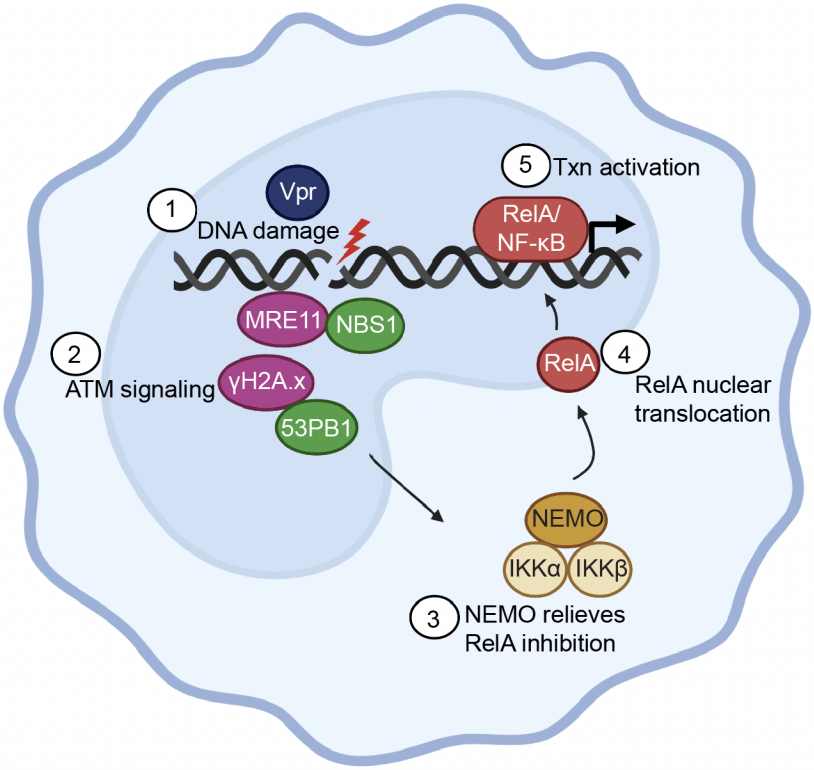
5 Txn activation
Vpr
1
DNA damage
RelA/
NF-κB
MRE11
NBS1
2
ATM signaling
γH2A.x
53PB1
RelA
4
RelA nuclear
translocation
NEMO
IKKα
IKKβ
3
NEMO relieves
RelA inhibition

822

823 **SUPPLEMENTAL FIGURE LEGENDS**

824

825 **Fig S1: Characterization of HIV-1 Vpr mutants S79A, H71R, and Q65R.** (A) Representative
826 western blot of 3X FLAG-Vpr WT and mutants from U2OS cells infected with rAAV expressing
827 Vpr WT, Q65R, H71R, S79A, or empty vector (EV) (negative control) as in Fig. 1A. α-tubulin
828 (loading control). Quantification of Vpr levels relative to corresponding α-tubulin and normalized
829 to Vpr WT. (B) Cell cycle arrest analysis of U2OS cell treated as in Fig. 1A. Percent of events in
830 G2 and G1 were measured using flow cytometry gating on mCherry positive cells (rAAV infection)
831 and stained for Hoescht (DNA content). N=3, one representative experiment shown. (C) Co-
832 immunoprecipitation against 3X FLAG-Vpr WT and mutants, probed for endogenous DCAF1,
833 from U2OS cells infected under the same conditions as Fig. 1A. Quantification of DCAF1
834 immunoprecipitated with Vpr WT and mutants relative to light chain. N=3, one representative
835 experiment shown. (D) Representative immunofluorescence images of U2OS cells infected under
836 the same conditions as Fig. 1A. Cells were either permeabilized then fixed or fixed and then
837 permeabilized. Vpr FLAG (orange) and DAPI (blue). Representative images taken at 24 hpi at
838 63x magnification. N=3, one representative experiment shown. Related to Figures 1-5.

839

840 **Fig S2: Vpr alters cellular transcription through diverse mechanisms that are either**
841 **dependent or independent of cell cycle arrest.** (A) Gene ontology using Metascape displaying
842 TRRUST analysis for upregulated genes. (B) Principal component analysis (PCA) of the RNA-
843 seq data showing the relatedness of the three biological replicates compared to empty vector or
844 untreated cells. (C) Protein-protein Interaction Enrichment Analysis using Metascape of the
845 shared downregulated genes among Vpr WT, S79A and H71R. Related to Figure 1.

846

847 **Fig S3: Vpr-induced DNA damage activates markers of ATM signaling.** (A) Live-cell imaging
848 taken on the IncuCyte of U2OS NBS1-GFP or 53PB1-GFP cells infected as in Fig. 1A for 56 hrs.
849 Heatmap displays NBS1 and 53PB1 mean fluorescence activity (MFI) (green) as arbitrary units
850 (AU). N=2, one representative experiment shown. (B & C) Quantification of DNA damage induced
851 in the live-cell imaging experiment in Fig. 3A at 8, 26, 33, and 48hpi. Foci per cell and foci size
852 were quantified using ImageJ software. Images were taken at 63x magnification using the LSM
853 900. N=3, one representative experiment shown with at least 50 cells per condition. Arbitrary units
854 (AU) displayed. Asterisk indicate statistical significance compared to untreated cells (negative
855 control) at the corresponding timepoint, as determined by one-way ANOVA test (NS,
856 nonsignificant; * P<0.03, ** P < 0.005, *** P< 0.0003, **** P< 0.0001). Related to Figure 3.
857
858 **Fig S4: Nemo knockout and NEMO-Binding inhibitor peptide (NBD) comparably inhibit Vpr-**
859 **induced NF-kB activation.** (A) qRT-PCR for Vpr expression of U2OS cells infected as in Fig. 4
860 in U2OS parental or NEMO knockout cells with technical triplicates. (B) Representative images
861 of U2OS parental or NEMO knockout cells infected as in Fig. 1A displaying γH2A.x (magenta),
862 3X FLAG-Vpr (yellow), DAPI (blue). Representative images taken at 24hpi at 63x magnification.
863 N=3, one representative experiment shown. (C) qRT-PCR of BIRC3 and CXCL8 in NEMO
864 knockout cells in the presence of Nemo-Binding inhibitor peptide (NBD, +) or the NBD negative
865 control peptide (-) at 36 hpi. Cells were treated under the same conditions as Fig. 4. Normalized
866 expression to GAPDH. N=3, one representative experiment shown. Asterisk indicate statistical
867 significance compared to NBD negative control, as determined by one-way ANOVA test (NS,
868 nonsignificant; * P< 0.003, *** P< 0.0003). Related to Figure 4.
869
870 **Fig S5: Infection of primary MDMs with VLPs packaging Vpr protein upregulates NF-κB**
871 **transcription dependent on NEMO.** (A) Flow cytometry plots displaying differentiation of PBMC-
872 derived monocytes to macrophages. Primary MDMs are CD14+, CD45+ and CD16+. N=4 one

873 representative experiment shown. (B) qRT-PCR for BIRC3 of MDMs treated with NBD inhibitor
874 peptide as in Fig. 5C with TNFα as positive control. N=3, displaying mean of 3 separate donors.
875 Asterisk indicate statistical significance compared to NBD negative control, as determined by one-
876 way ANOVA test (NS, nonsignificant; * P< 0.003, **** P< 0.0001). Related to Figure 5.
877
878 **Fig S6: HIV-1 infection of primary human MDMs upregulates NF-κB transcription and is**
879 **rescued by Vpr.** (A) Histogram quantifying percent of infected MDMs with HIV-1 ΔEnv at 48hpi.
880 N=4, one representative experiment shown. (B) qRT-PCR for unspliced HIV-1 RNA at 8, 16, 24
881 and 48hpi. N=4, one representative experiment shown. (C) qRT-PCR for BIRC3 or CXCL8 of
882 MDMs infected with HIV-1 ΔEnv at 8, 16, 24 and 48hpi in four separate donors. N=4. (D)
883 Histogram quantifying percent of infected MDMs with HIV-1, HIV-1ΔVpr, HIV-1ΔVpr +Vpr, mock
884 or untreated at 48hpi. N=3, one representative experiment shown. (E) qRT-PCR for BIRC3 of
885 MDMs infected with MOI 5U/mL of HIV-1, HIV-1 ΔVpr, HIV-1 ΔVpr +Vpr WT viruses or mock.
886 Displaying the mean of three separate donors. Normalized expression to GAPDH. Asterisk
887 indicate statistical significance compared to untreated negative control, as determined by Welch
888 t-test for BIRC3 (NS, nonsignificant; * P<0.04). (F) qRT-PCR for BIRC3 or CXCL8 of MDMs
889 infected with HIV-1, HIV-1ΔVpr, HIV-1ΔVpr +Vpr, mock at 8hpi from three separate donors. One
890 representative experiment shown with technical triplicates. Asterisk indicate statistical
891 significance compared to untreated control, as determined by one-way ANOVA test (NS,
892 nonsignificant; * P< 0.003, ** P< 0.001). Related to Figure 6.
893
894 **Files S1 & S2: HIV-1 Vpr WT and mutants alter cellular transcription.** Analysis of all
895 upregulated (File S1) and downregulated (File S2) genes in the RNA seq analysis that passes
896 statistical significance of Log2 (1.25), p < 0.01, and FDR < 4.50E-05. Counts per million reads
897 mapped (CPM) Log2 fold changes were calculated relative to untreated control. Related to
898 Figure 1 and Figure S2.

899

900 **Table 1. HIV-1 Vpr WT and mutant phenotypes.** (+) indicates a phenotype conferred by Vpr, (-

901) indicates a phenotype not conferred by Vpr, and (-/+) indicates an intermediate Vpr phenotype.

	Localization as WT	Cell Cycle Arrest	Engages DCAF1	DNA Damage	NF-kB activation
HIV-1 Vpr WT	+	+	+	+	+
S79A	+	-	+	+	+
H71R	+	-	- / +	+	+
Q65R	-	-	-	-	-

902

Fig S1.

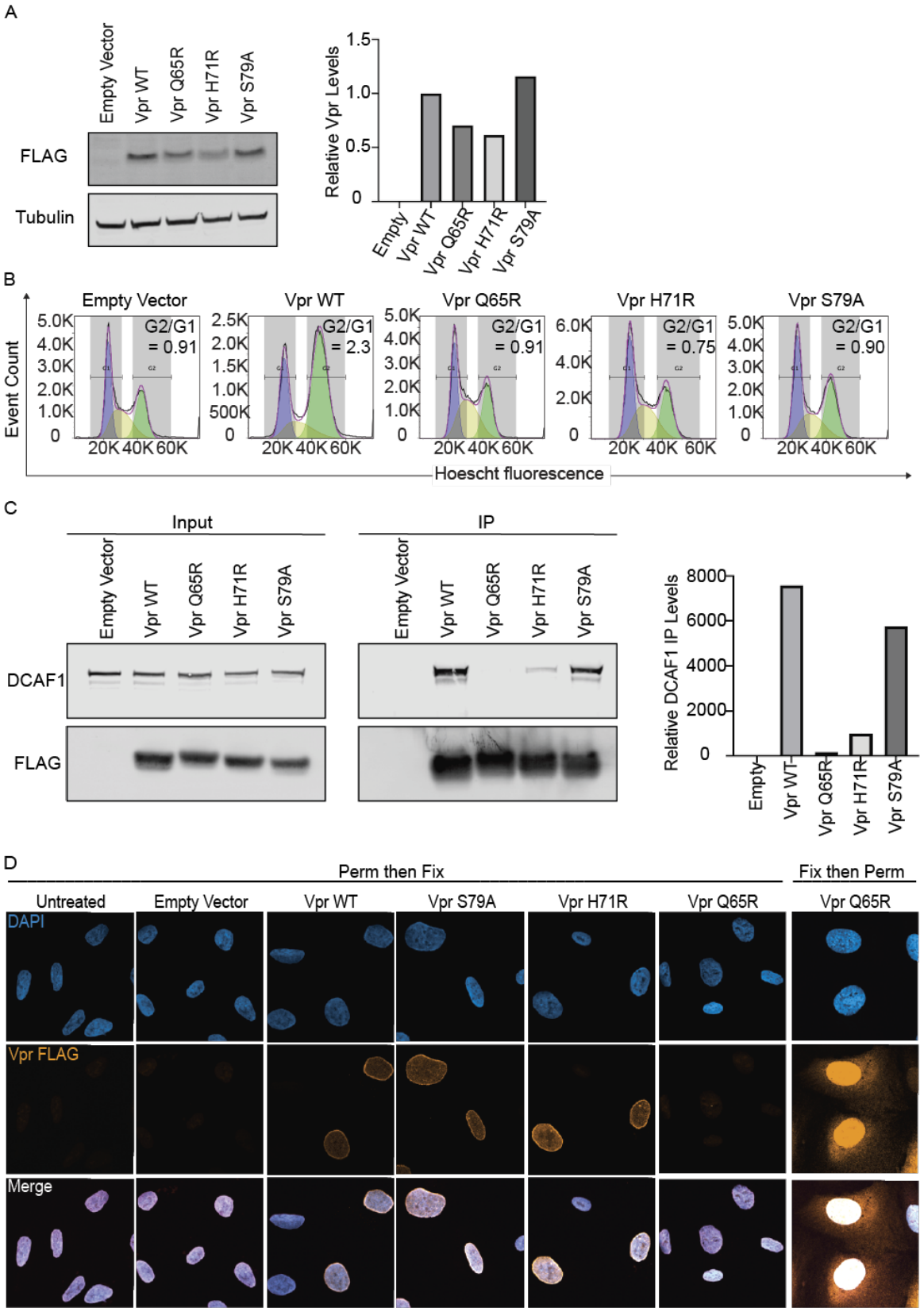
A
Empty Vector
Vpr WT
Vpr Q65R
Vpr H71R
Vpr S79A
FLAG
Tubulin
Relative Vpr Levels
1.5
1.0
0.5
0
Empty
Vpr WT
Vpr Q65R
Vpr H71R
Vpr S79A
B
Empty Vector
Vpr WT
Vpr Q65R
Vpr H71R
Vpr S79A
G2/G1 = 0.91
G2/G1 = 2.3
G2/G1 = 0.91
G2/G1 = 0.75
G2/G1 = 0.90
Event Count
20K 40K 60K
Hoescht fluorescence
C
Input
IP
DCAF1
FLAG
Relative DCAF1 IP Levels
8000
6000
4000
2000
0
D
Perm then Fix
Fix then Perm
Untreated
Empty Vector
Vpr WT
Vpr S79A
Vpr H71R
Vpr Q65R
Vpr Q65R
DAPI
Vpr FLAG
Merge

Fig S2.

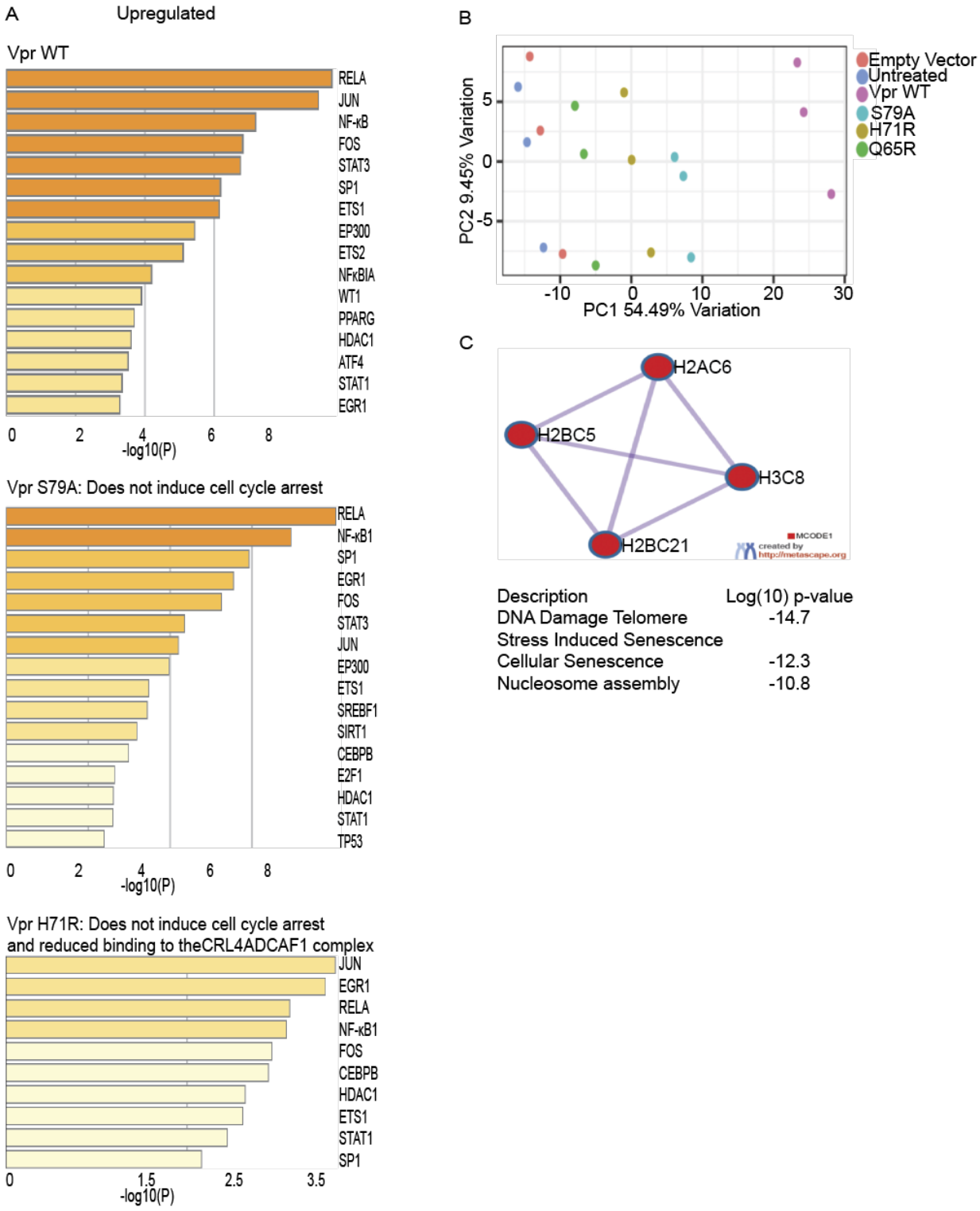
A
Upregulated
Vpr WT
RELA
JUN
NF-κB
FOS
STAT3
SP1
ETS1
EP300
ETS2
NFκBIA
WT1
PPARG
HDAC1
ATF4
STAT1
EGR1
0
2
4
6
8
-log10(P)
Vpr S79A: Does not induce cell cycle arrest
RELA
NF-κB1
SP1
EGR1
FOS
STAT3
JUN
EP300
ETS1
SREBF1
SIRT1
CEBPB
E2F1
HDAC1
STAT1
TP53
0
2
4
6
8
-log10(P)
Vpr H71R: Does not induce cell cycle arrest
and reduced binding to theCRL4ADCAF1 complex
JUN
EGR1
RELA
NF-κB1
FOS
CEBPB
HDAC1
ETS1
STAT1
SP1
0
1.5
2.5
3.5
-log10(P)
B
Empty Vector
Untreated
Vpr WT
S79A
H71R
Q65R
PC2 9.45% Variation
5
0
-5
-10
0
10
20
30
PC1 54.49% Variation
C
H2AC6
H2BC5
H3C8
H2BC21
MCODE1
created by
http://metascape.org
Description
Log(10) p-value
DNA Damage Telomere
-14.7
Stress Induced Senescence
Cellular Senescence
-12.3
Nucleosome assembly
-10.8

Fig S3.

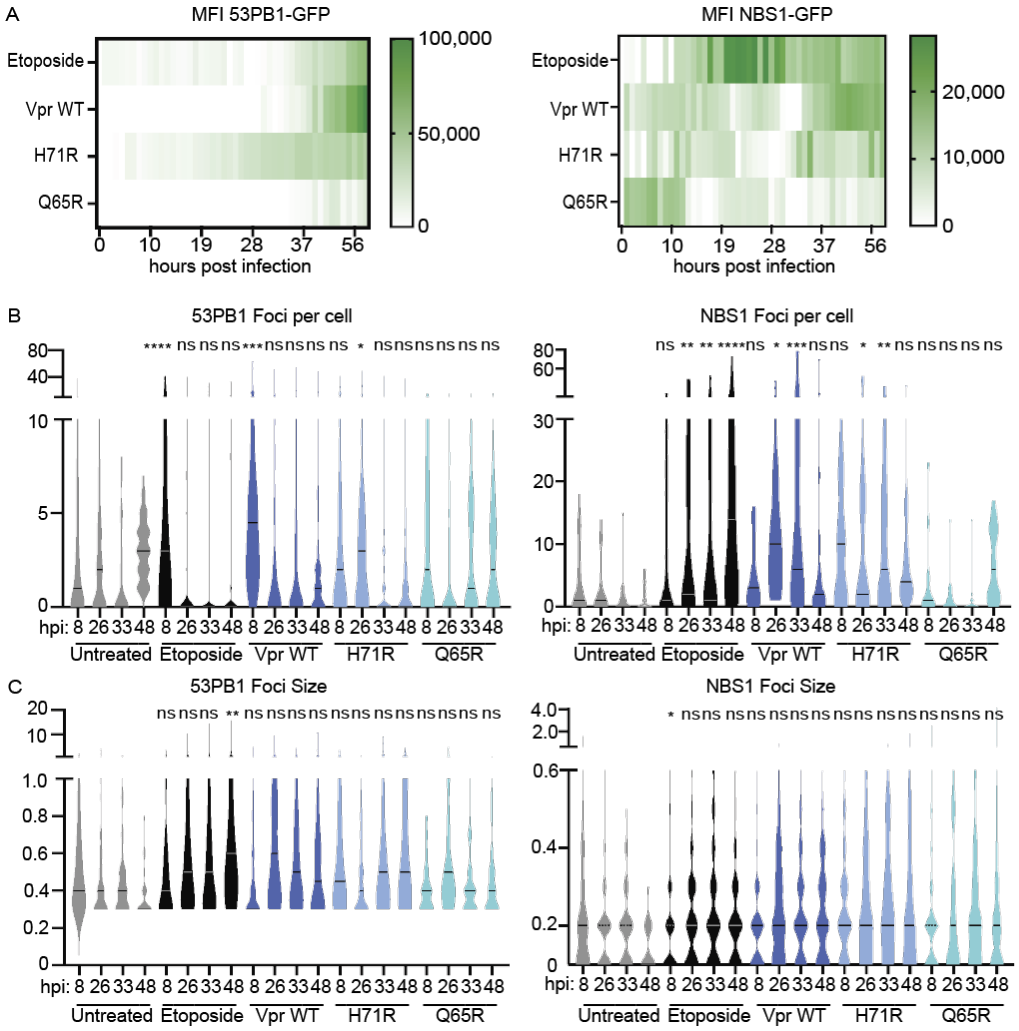
A
MFI 53PB1-GFP
Etoposide
Vpr WT
H71R
Q65R
100,000
50,000
0
0 10 19 28 37 56
hours post infection
MFI NBS1-GFP
20,000
10,000
B
53PB1 Foci per cell
NBS1 Foci per cell
hpi: 8 26 33 48 8 26 33 48 8 26 33 48 8 26 33 48 8 26 33 48
Untreated Etoposide Vpr WT H71R Q65R
C
53PB1 Foci Size
NBS1 Foci Size

Fig S4.

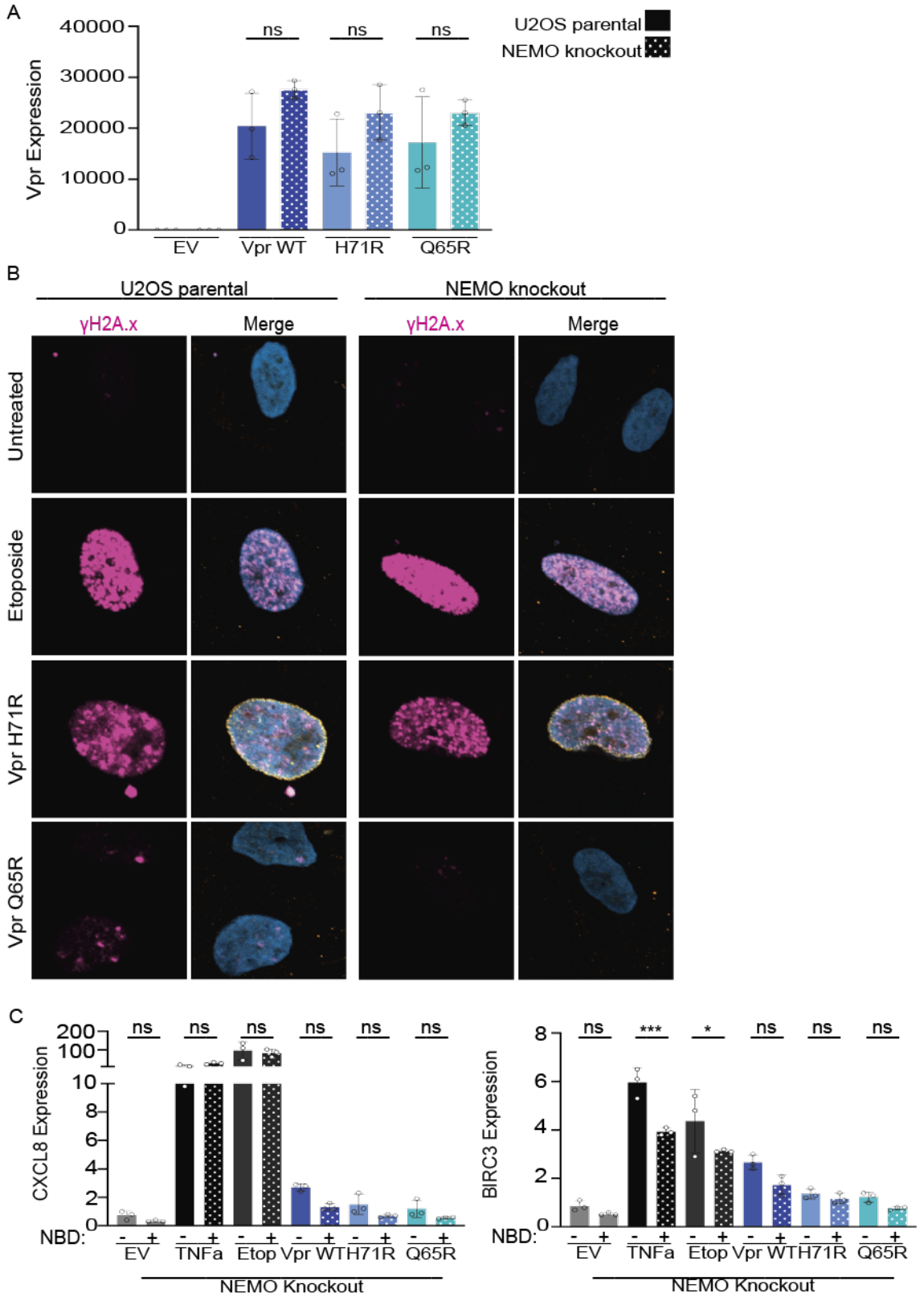
A
Vpr Expression
40000
30000
20000
10000
0
ns
ns
ns
U2OS parental
NEMO knockout
EV
Vpr WT
H71R
Q65R
B
U2OS parental
NEMO knockout
γH2A.x
Merge
γH2A.x
Merge
Untreated
Etoposide
Vpr H71R
Vpr Q65R
C
CXCL8 Expression
200
100
10
8
6
4
2
0
ns
ns
ns
ns
ns
ns
NBD:
EV
TNFa
Etop
Vpr WT
H71R
Q65R
NEMO Knockout
BIRC3 Expression
8
6
4
2
0
ns
***
*
ns
ns
ns
NBD:
EV
TNFa
Etop
Vpr WT
H71R
Q65R
NEMO Knockout

912 **Fig S5.**

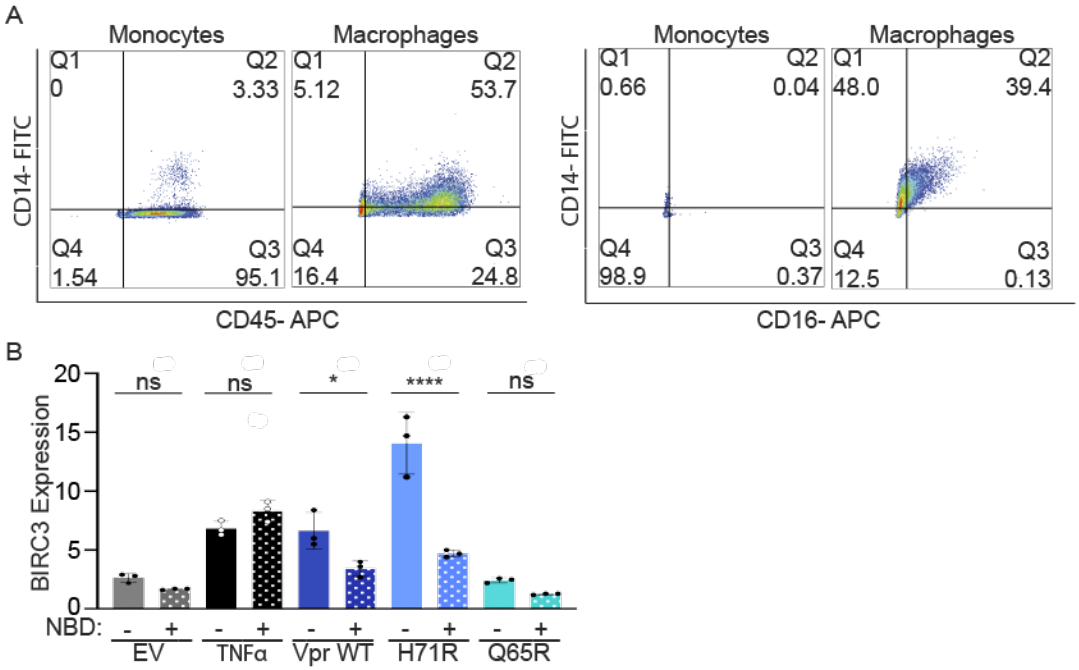

913

914 **Fig S6.**

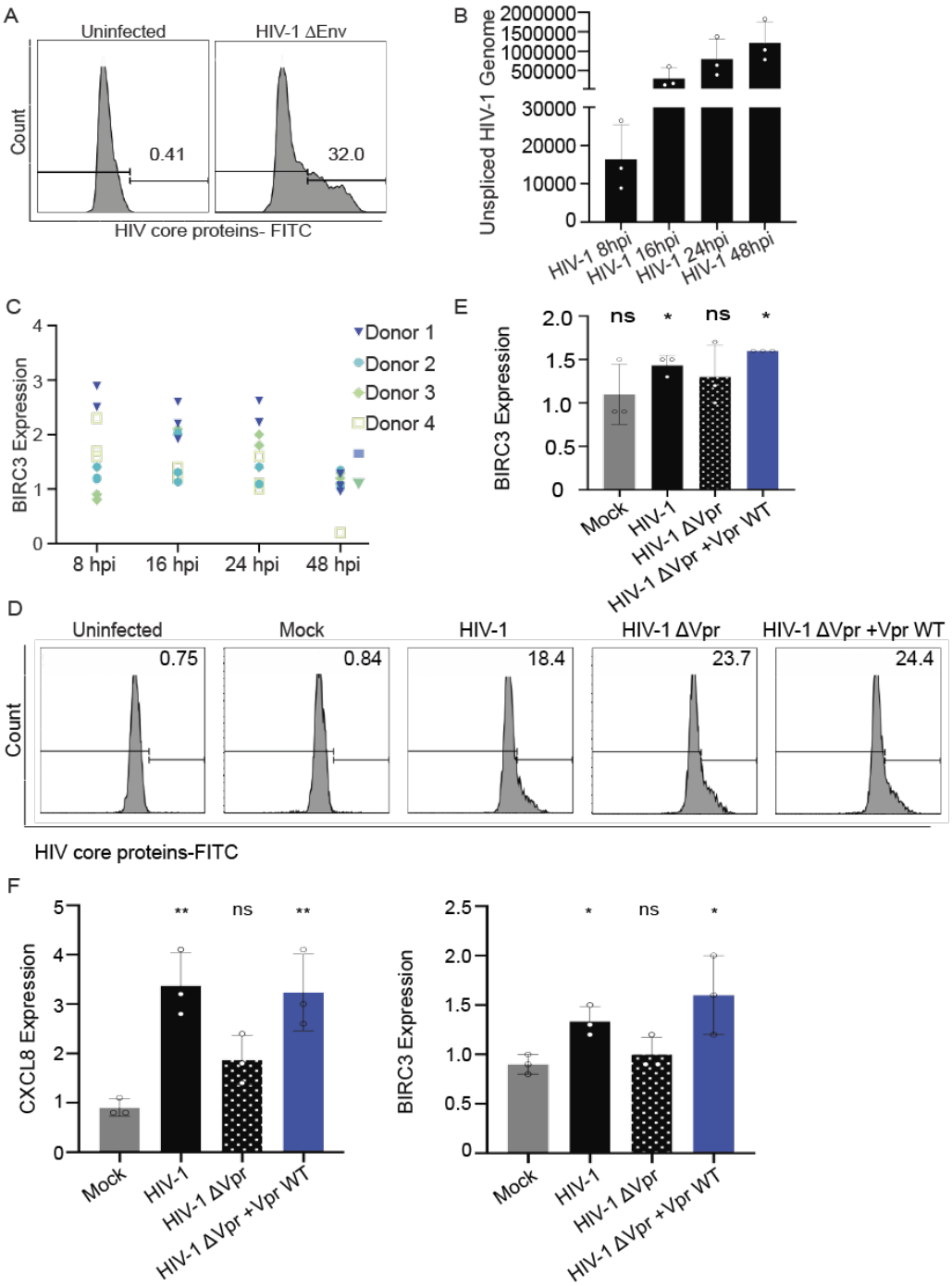

915